# PROTEOMIC ASSESSMENT OF POST-TRANSLATIONAL MODIFICATIONS IN THE BRAIN OF *5X-FAD* FEMALES

by

Matthew Gonzales



A Thesis Submitted to the Faculty of the

GRADUATE INTERDISCIPLINARY PROGRAM IN PHYSIOLOGICAL SCIENCES

In Partial Fulfillment of the Requirements

For the Degree of

MASTER OF SCIENCE

In the Graduate College

THE UNIVERSITY OF ARIZONA

2024

THE UNIVERSITY OF ARIZONA
GRADUATE COLLEGE

As members of the Master's Committee, we certify that we have read the thesis prepared by Matthew Gonzales, titled *Proteomic Assessment of Post-Translational Modifications in the Brain of 5x-FAD Females* and recommend that it be accepted as fulfilling the dissertation requirement for the Master's Degree.

*Paulo W. Pires, Ph.D.* Date: 6/5/2024

*Paul R. Langlais, Ph.D.* Date: 20240605

*Dawn K. Coletta, Ph.D.* Date: 6/5/2024

Final approval and acceptance of this thesis is contingent upon the candidate's submission of the final copies of the thesis to the Graduate College.

I hereby certify that I have read this thesis prepared under my direction and recommend that it be accepted as fulfilling the Master's requirement.

*Paulo W. Pires, Ph.D.* Date: 6/5/2024
Master's Thesis Committee Chair
*Department of Physiology*

## ACKNOWLEDGEMENTS

This research and thesis would not have been a reality without the unwavering support and guidance of my committee members. I wish to express my sincere appreciation to my mentor, Dr. Paulo Pires, for allowing me the opportunity to practice science in a positive and encouraging environment. If it were not for his understanding, I would not have had the chance to appreciate the life lessons that the last two years have shown me. Thank you for helping me develop as a scientist, a critical thinker, and a problem solver. Also, my gratitude is extended to our Postdoctoral Researcher, Dr. Josiane Fernandes Da Silva, as this project was her design and her enthusiastic instruction allowed myself to assist seeing the research through. Additionally, I would like to thank my committee members, Dr. Paul Langlais, for keeping me from diving down the infinite rabbit holes that is proteomics and bioinformatics, and Dr. Dawn Coletta, for being the strongest advocate for the pursuit of knowledge in its most selfless form a student could ask for. It is through the assistance of you all that I earn this graduate degree.

Moreover, the backing of my mother, father, sister and brother have been integral in my pursuit of higher education. You have shown me nothing but love and consideration, and I hope you understand the pride I have in our family. Thank you for teaching me to appreciate the small and large endeavors in life.

To my friends that have lifted me up these last two years, thank you for reminding me of where I come from and what is important in life.

## TABLE OF CONTENTS

## List of Figures

## List of Appendices & Supplemental Figures

**Abstract**

Dementia prevalence is expected to more than double in the next three decades stressing numerous healthcare systems and caregivers across the globe. Alzheimer's disease (AD), the most common form of dementia, is a multi-factorial neurodegenerative disease without a cure due to the incomplete understanding of its complex progression. Our aim is to report hypothesis generating data for targeted functional studies to understand the mechanisms underlying differential expression and post-translational modifications in AD using the 5x-FAD murine model. The bulk proteome, S-nitrosylated proteome, phosphoproteome, and acetylome were assessed by unbiased tandem mass spectrometry and label-free quantitative proteomics. Affinity purification assays were utilized to enrich samples to evaluate S-nitrosylated proteins. Western blots analysis was performed on specific protein targets of interest from the bulk proteome and S-nitrosylated proteome to validate proteomic results. We observed 426 proteins with differential expression patterns across the whole proteome and 225 proteins with alterations in S-nitrosylation in 6-monthold female 5x-FAD mice. Additionally, 161 phosphopeptides and 23 acetylated peptides were found to be significantly different compared to wild-type (WT) littermates. Gene ontology (GO) analysis implicated enrichment of glutamateric signaling, oxidoreudctase activity, and cytoskeletal proteins, supporting current AD literature, while also elucidating the novel targeting that post translational modifications could have on the electron transport chain, transcription, and histone and mitochondrial acetylation. We further show primary validation of increased glial fibrillary acidic protein expression patterns, known to occur in AD patients, and revealed a conserved decrease in S-nitrosylation of myelin proteolipid protein. However, myelin-associated oligodendrocyte basic protein quantification did not allow for conclusive inferences to an under investigated aspect of AD. These proteomic data concur with well-documented protein changes, post-translational modifications, and enriched signaling pathways found in humans living with AD and animal models of the disease, linking specific proteins involved with cytoskeletal organization, mitochondrial ATP genesis, ion homeostasis, transcription, translation, and myelin sheath maintenance contributing to the multifactorial nature of AD.

## Introduction

Dementia is an encompassing term for diseases that affect memory and higher order processing in the brain. Globally, over 55 million people live with dementia, and these progressive afflictions mainly affect those 65 years or older [1]. Over ten percent of dementia patients reside in the United States with this number projected to more than double by 2050 [2]. In 2023, the nation spent nearly $345 billion in care for dementia patients, a number estimated to reach $1 trillion in the next three decades [3]. While the percentage of individuals 65 years or older is increasing across the nation, Arizona claims a percentage that is higher than the national average [4]. Dementia, in all its forms, continues to be a socioeconomic and healthcare problem not only at the state and national level, but on a global scale as life expectancy continues to increase. While patients can be affected by more than one type of dementia, the most common form is Alzheimer's disease [5].

Alzheimer's disease (AD) is a progressive, neurodegenerative condition that is characterized by the abnormal aggregation of the amyloid-β peptide (Aβ) and neurofibrillary tangles composed of hyperphosphorylated tau. Aβ is generated after cleavage of the membrane-bound amyloid-beta precursor protein (AβPP) from neuronal membranes, and distinct cleavage sites can lead to accumulation of different Aβ peptides [6]. $A\beta_{40}$ is the is the most plentiful product within both the AD and normal aging brain, while $A\beta_{42}$ is known to have a higher toxicity, yet is not as abundant [7]. Both peptide species are able to form organized amyloid fibril aggregates that contribute to the framework within Aβ plaques [8]. AD is also associated with hyperphosphorylation of the microtubule stabilizing protein, tau [9]. Physiologically, tau proteins contribute to maintaining neuronal cell framework; however, in AD, dissociation of tau from microtubules leads to neurofibrillary tangles (NFTs) accumulating within the cell [10]. AD progression involves worsening of these pathological hallmarks; however, several other age-related alterations are simultaneously occurring that can exacerbate the patient's condition as well as potentiate each other. These changes include cerebral microvascular dysfunction, inflammation, increased reactive oxygen species production, and mitochondrial dysfunction [11-14]. For this reason, along with prevalence projections, it is essential that animal models accurately recapitulate the physiological effects experienced by humans.

The brain is a highly metabolic organ, consuming 20 percent of circulating oxygen and nutrients at rest and up to 50 percent during higher executive function, with little capacity for nutrient storage [2]. Neuronal function requires constant supply of nutrients to maintain electrochemical communication. In addition, their metabolites are disposed by the brain microvasculature and glymphatics circulation, and their microenvironment is regulated by a highly heterogenous population of glial cells [15-17]. This complex environment is therefore heavily dependent on the communication between neurons, glia, smooth muscle cells, and the endothelium to properly respond to metabolic activity. The cerebral microvasculature functions to equitably supply local regions of the brain with the essential fuel and oxygen based on metabolic demand in real time. This homeostatic mechanism is referred to as neurovascular coupling. Neurovascular coupling is attenuated in aging individuals, underlying normal cognitive decline, and is mediated by loss of endothelium and smooth muscle dysfunction [18, 19]. The decreased ability to supply neurons with proper nourishment and removal of parenchymal Aβ is a key source of neuroinflammation and reactive oxygen species production [19, 20].

Reactive oxygen species (ROS) are broadly defined as molecules that contain an oxygen atom while also possessing one or more unpaired electrons that readily react with other molecules [21]. Notable ROS include superoxide and hydrogen peroxide and are produced in small quantities from mitochondrial respiration and inflammation [22, 23]. At these low levels, ROS molecules play a role in several cell signaling pathways such as differentiation, cell survival, and cytoprotection [21-24]. However, when ROS levels become elevated, these radicals are known to induce senescence and apoptosis [11, 25]. Therefore, ROS molecules are thought to be involved in the natural aging process as well as numerous pathologies if their regulation becomes imbalanced [11]. In AD, ROS production is elevated to the point where they overwhelm endogenous antioxidant mechanisms, thus leading to neuronal damage [26]. Aβ aggregates are known to sequester metals such as zinc, copper, and iron, leading to these senile plaques becoming an additional source of oxidative stress in AD [27]. Along with their cell signaling capabilities, ROS can cause lipid peroxidation, DNA damage, and protein oxidation [18, 22, 25, 28]. These reactions and their end-products can bind to and alter the function of many biomolecules, potentially exacerbating ROS production and further compounding on the natural aging process and neurodegeneration [22, 29].

The brain's consumption of at least 20% of the body's oxygen leads to the production of ROS in an organ with increased risk for molecular damage compared to others (15). Existing endogenous antioxidant compounds can maintain oxidant levels in a homeostatic range, however, pathological insults can increase ROS to overwhelming levels. The two main categories of antioxidant defense are enzymatic and non-enzymatic antioxidants (45). Enzymatic antioxidant mechanisms are useful in maintaining intracellular concentrations of ROS, but when abnormal levels are reached, these enzymes have a limited ability to keep up with their substrates due to membrane permeability and biochemical rate constants (49). Non-enzymatic antioxidants have been shown to have beneficial effects on pathological markers of AD and cognition in rodents and humans, but dosage and bioavailability of these ROS scavengers have made treatment plans difficult (45). Without efficient antioxidant systems, ROS are able to react with physiological oxidants such as nitric oxide, exacerbating the pathology.

Nitric oxide (NO) can interact with superoxide ions forming peroxynitrite, which at low levels can form nitrate ions that are known to not have detrimental effects (49). At high levels, peroxynitrite can nitrate proteins causing irreversible damage, degradation, and loss of function seen in AD (18, 19, 25, 26). It has been shown in AD rodent models, that increased concentrations of superoxide, due to high metabolic activity or increased oxidative stress, reacts with NO within the brain and reduces the levels of bioavailable NO leading to decreases in the compound's neuroprotective effects (13, 49).

Two constitutive nitric oxide synthase (cNOS) enzymes are expressed in the brain: neuronal nitric oxide synthase (nNOS) and endothelial nitric oxide synthase (eNOS) [24]. A third isoform's expression can be activated by inflammatory cytokines and is known as inducible nitric oxide synthase (iNOS) [30, 31]. nNOS has a prominent role in neuronal communication, both by promoting long-term potentiation and inhibition through nitrergic interneurons. eNOS is highly expressed by endothelial cells and acts as an inhibitor of leukocyte and platelet aggregation and adhesion. Microglia, astrocytes, neurons, vascular smooth muscle cells, and endothelial cells can have iNOS expression induced due to inflammatory cytokines. Both cNOS isozymes function to regulate vascular tone, blood pressure, and vasomotion within the brain microvasculature, whereas NO derived from iNOS can halt activity of key metabolic enzymes in the mitochondria and fragment genetic material of invading microbes [30]. nNOS and eNOS are calcium dependent and

increase their NO production following activation of $Ca^{2+}$-calmodulin complex binding. However, iNOS is calcium-independent and produces NO over hours at a time, in a substrate-dependent manner, and chronic iNOS expression leads to NO overproduction, resulting in increased concentrations of peroxynitrite [24]. eNOS expression decreases in normal aging and AD leading to the uncoupling of the enzyme and could contribute to vascular dysfunction in AD rodent models and humans living with the disease [31]. Glutamate signaling, the primary excitatory neurotransmitter in the central nervous system, increases intracellular calcium through NMDA receptors causing increased NO production [32, 33]. Amyloid fibrils in the extracellular space of the brain are known to decrease glutamate uptake by neurons and increase glutamate release by astrocytes causing excitotoxicity, a characteristic believed to contribute to AD progession [33]. Although uncoupling and hyperactivity of these three isozymes leads to inefficient NO production and sporadic superoxide, a physiological function of the compound is the post-translational binding of NO to proteins which is known as S-nitrosylation. This post-translational modification (PTM), along with others, alters protein function that may be different in a pathological state from normal physiological action [24, 30, 31, 34, 35].

For two decades proteomic technologies have been leveraged to uncover differential proteins expression patterns in the AD brain [36, 37]. These results have been useful in beginning to understand structural and survival changes that the numerous cells within the brain employ in response to this condition [38, 39]. Initial studies found that heat shock, antioxidant, proteolytic, and signal transducing protein expression were among the most affected [37, 38]. Further experiments sought to focus on the proteome of amyloid plaques to understand how this AD biomarker can promote different phenotypes of surrounding cells and regions of the brain that are highly vulnerable to oxidative stress such as the hippocampus [36, 40, 41]. These studies have aided the search for the extent that increased oxidative stress had on cytosolic and metabolic molecules as they yielded numerous proteins that were oxidized or peroxidized due to metabolites of these amyloid plaques. The literature on the oxidation of proteins in varying organelles and spaces of cells that make up or surround the brain has become extensive and is still growing [42]. These findings provided a foundation of data that has since been used to appreciate the compounding effects of neuroinflammation and differential glutamate signaling in the progression of AD [37, 40, 42]. Although these necessary steps have been made to advance comprehension of this neurodegenerative disease, current therapeutics for patients are limited in options and efficacy,

expensive and can have detrimental effects. Therefore, in the last ten years, finding proteins with alterations in PTMs in response to AD has received growing interest. Recently, S-nitrosylated proteins have been found to be altered in AD models and humans [35, 43]. This modification has been speculated to have an indirect function of blocking proteins from irreversible or damaging PTMs [44]. Large scale PTMs, such as phosphorylation, compile most of the current literature they can be easily assessed using mass spectrometry without the need of affinity purification assays [36, 38]. Novel, more selective PTMs, such as S-nitrosylation, have allowed for "subproteomic" profiles that are currently being investigated. Elucidating the outcome these alterations have on downstream effectors will allow for a holistic understanding of AD and potentially valuable therapeutic targets.

Our current study sought to search for novel changes in protein expression patterns and post-translational modifications of proteins in the brain cortex of 6-month-old female *5x-FAD* mice using unbiased *in tandem* mass spectrometry. S-nitrosylation was measured following an affinity purification assay of cortical lysates. Phosphorylation and acetylation data were obtained through bioinformatics analysis of the bulk proteome from these different lysates. Secondary validation of proteins targets of interest was performed using Western blot techniques. Protein expression, S-nitrosylation, phosphorylation, and acetylation levels were analyzed against age-matched wild-type littermates.

## Methods

### *Animals*

All animal procedures in this study were approved by the Institutional Animal Care and Use Committee of the University Of Arizona College Of Medicine (IACUC Protocol No. 18-473) and are in accordance with the National Institutes of Health's *Guide for the Care and Use of Laboratory Animals.* The *5x-FAD* transgenic mouse model was purchased from Jackson Laboratory and these transgenic AD mouse model co-expresses five mutations associated to Familial Alzheimer's disease (FAD). Three mutations, K670N/M671L (Swedish), I716V (Florida), and V717I (London) are expressed in the *APP* gene and two mutations, M146L and L286V, are expressed in the *PSEN1* gene. Overexpression of these genes specifically in the brain is due to these genes being under the neuronal-specific *Thy1* promoter. Young mice (6-month old) used in these studies were acquired by breeding *5x-FAD* mice originally purchased from Jackson Laboratory (strain number 34840-JAX) and are now maintained in our breeding colony at the University of Arizona. All mice were bred using a C57BL/6 background and wild-type (WT) littermates were used as controls. Animals were housed in the animal facilities at the University of Arizona with a maximum of four mice per cage to maintain social interactions. Cages were stored in rooms with controlled environmental conditions with 12-h:12-h light/dark cycle and had free access to commercial rodent chow and water.

### *Sample Preparation*

Protein expression was measured using 50 mg of brain cortex tissue that was homogenized in 500 µL Buffer A containing a blocking reagent from a biotin-switch kit used for detection of S-nitrosylated proteins to lyse cells and block free thiol groups (*Cayman Chemical*, Ann Arbor, MI, catalog# 10006518). Protease inhibitors were also added to the homogenates and the samples were incubated for 30 minutes with gentle agitation. Homogenates were then centrifuged for 10 minutes at 4ºC 15,000xg. Supernatant was then separated into two aliquots and incubation with acetone for an hour at -20ºC was used to precipitate proteins. Samples were then centrifuged for 10 minutes at 4ºC 3,000xG, acetone was removed, and pellet from one aliquot was resuspended in Buffer B from biotin-switch kit. This sample was aliquoted into two tubes again. One aliquot would be used as a

control to measure contribution of endogenous biotinylated proteins following affinity purification and the other would be utilized for protein quantification and measuring protein expression at the whole proteome level. The second aliquot from the initial sample would have its pellet resuspended in Buffer B with reducing and labeling reagents. This solution reduces S-nitrosylated thiol groups resulting in free thiols that are then covalently bound by maleimide-biotin molecules. This process will allow for indirect measurement of S-nitrosylated proteins. After incubation for an hour at room temperature, the solution was removed, and acetone was used to precipitate proteins once more. Lasty, after acetone removal, a wash buffer was used for pellet resuspension. The samples to measure endogenous biotinylated proteins and S-nitrosylated proteins were used for an affinity purification assay and samples used for protein quantification were utilized for Western blot and quantitative proteomics.

### *BCA Protein Quantification*

Twenty (20) µL of sample were used to quantify protein concentrations according to manufacturer's recommendations, as previously described [39], using the Bicinchoninic Acid (BCA) method (ThermoScientific, catalog# 23225, Pierce BCA Protein Assay Kit).

### *Affinity Purification*

To isolate endogenously biotinylated/S-nitrosylated proteins, 500 µg of resuspended proteins were transferred to a 1.5 mL tube and a final volume of 200 µL was obtained by supplementation with PBS containing protease inhibitors (*Sigma-FAST*, catalog# S8820). After addition of 30 µL of streptavidin-coated metal beads (*ThermoFisher Scientific*, catalog# MSPB-6003-74), the sample was incubated for four hours at 4ºC with gentle agitation. Following incubation, samples were added to a magnetic base (*DynaMag-2*, catalog# 12321D, Invitrogen), to pull biotin labeled proteins out of solution. Samples were washed three times with wash buffer and underwent Western blot protocol described below.

***Western Blot***

Proteins were denatured with 2x Laemmeli buffer (4% SDS, 20% glycerol, 10% 2-mercaptoethanol. 0.004% bromophenol blue, and 0.125M Tris HCl, pH 6.8) and heated at 100ºC for 10 minutes. 50 µg of proteins were electrophoretically separated on 4-15% Mini-PROTEAN TGX Stain-Free precast gels (*Bio-Rad*, catalog# 4568083) with 10% SDS-PAGE buffer at 100 V for 1 hour. Proteins were transferred to a nitrocellulose membrane (*Bio-Rad*, catalog# 1620115) using electrophoresis at 100 V for 1.5 hours. After transferring, membranes were blocked with Tris buffed saline (TBS) containing 1% albumin and 0.01% Tween overnight at 4ºC. Membranes were then incubated with primary antibody overnight at 4ºC, washed 3x the following day with TBS-Tween, and incubated with specific secondary antibodies coupled with fluorescence for manufacturer recommended amount of time. Membranes were then imaged using ChemiDoc MP Imaging System (Bio-Rad Laboratories Inc, Hercules, CA).

***In-gel Digestion***

Fifty (50) µg of mouse cortical lysate was separated using SDS-PAGE and stained with Bio-Safe Coomassie G-250 Stain. Individual lanes of the SDS-PAGE gel were cut into 6 slices, placed in 0.6mL LoBind polypropylene tubes (Eppendorf, Hauppauge, NY), destained twice with 375 µL of 50% acetonitrile (ACN) in 40 mm $NH_4HCO_3$ and dehydrated with 100% ACN for 15 minutes. Gel slices were exposed to trypsin digestion and the resulting peptides were purified using C18-based desalting, as previously described [45]. In brief, ACN was aspirated and afterwards the gel pieces were dried in a vacuum centrifuge at 60ºC for 30 minutes. Trypsin (250 ng, Sigma-Aldrich) in 20 µL of 40 mM $NH_4HCO_3$ was added and the samples were held at 4ºC for 15 minutes prior to addition of 50-100 µL of 40 mm $NH_4HCO_3$. The digestion was permitted to proceed at 37ºC overnight and was terminated by the addition of 10 µL of 5% formic acid (FA). Following 30 minutes of incubation at 37ºC and centrifugation for 1 minute, each sample's supernatant was transferred to a clean LoBind polypropylene tube. This extraction protocol was repeated using 40 µL of 0.5% FA and the two extracts were combined and dried down to approximately 5-10 µL followed by addition of 10 µL of 0.05% heptafluorobutyric acid: 5% FA (v/v) and lastly, incubation at room temperature for 15 minutes. The remaining peptide mixtures were loaded on a solid phase C18 ZipTip (Millipore, Billerica, MA), washed with 35 µL of 0.005%

heptafluorobutyric acid: 5% FA (v/v), and eluted first with 4 µL of 50% CAN: 1% FA (v/v) and then a more stringent elution with 4 µL of 80% CAN: 1% FA (v/v). The eluates were combined and dried completely by vacuum centrifugation and 6µL of 0.1% FA (v/v) was added followed by sonication for 2 minutes. A final volume of 2.5 µL of sample was then analyzed using *tandem* mass spectrometry.

***Mass Spectrometry***

HPLC-ESI-MS/MS was performed in positive ion mode on a Thermo Scientific Orbitrap Fusion Lumos tribid mass spectrometer fitted with an EASY-Spray Source (Thermo Scientific, San Jose, CA) as previously described [46]. Briefly, nanoflow liquid chromatography was used without a trap column using Thermo Scientific UltiMate 3000 RSLCnano System with an EASY Spray C18 LC column (Thermo Scientific, 50 cm x 75 µm inner diameter, packed with PepMap RSLC C18 material, 2 µm, catalog# ES803): loading phase for 15 minutes at 0.300 µL/min: mobile phase, linear gradient of 1-34% Buffer B in 119 minutes at 0.220µL/min, followed by a step to 95% Buffer B over 4 minutes at 0.220µL/min, hold 5 minutes at 0.250 µL/min (total run 159 minutes): Buffer A = 0.1% FA/$H_2O$: Buffer B =0.1% FA in 80% CAN. All solvents were liquid chromatography mass spectrometry grade. Spectra were obtained using XCalibur, version 2.3 (Thermo Scientific). A "top speed" data-dependent MS/MS analysis was performed. Dynamic exclusion was enabled with a repeat count of 1, repeat duration of 30 seconds, and an exclusion duration of 60 seconds.

***Label-free Quantitative Proteomics***

Progenesis QI for proteomics software (version 2.4, Nonlinear Dynamics Ltd., Newcastle upon Tyne, UK) was used to perform ion-intensity based label-free quantification as previously described [46]. Briefly, in an automated format, .raw files were imported and converted into two-dimensional maps (y-axis = time, x-axis = m/z) followed by selection of a reference run for alignment purposes. Aggregate data sets with all peak information from each sample were created from the aligned runs. This was further narrowed down by selecting only +2, +3, and +4 charged ions for further analysis. A peak list of fragment ion spectra from strictly the top ten most intense

precursors of a feature was exported in Mascot generic file (.mgf) format and examined against the 202301 Swissprot *Mus musculus* database (17148 entries) using Mascot (Matrix Science, London, UK: version 2.4). Search variables that were used were: 10 ppm mass tolerance for precursor ion masses and 0.5 Da for product ion masses; digestion with trypsin: a maximum of two missed tryptic cleavages; variable modifications of oxidation of methionine and phosphorylation of serine, threonine, and tyrosine: $^{13}C=1$. The subsequent Mascot .xml file was imported into Progenesis, permitting peptide/protein assignment, while peptides with a Mascot Ion Score of less than 25 were not considered for further analysis. Mass spectrometry proteomics data have been deposited to the ProteomeXchange Consortium (PMID 27924013) via the PRIDE partner repository with the dataset identifier PXD000XYZ and 10.0XYZ/PXD000XYZ.

Perseus [47, 48] was utilized for production of unbiased hierarchal clustering analysis (heat map) and cluster profile plots. Gene ontology and Reactome pathway enrichment analysis was performed with DAVID [49].

## Results

### *Proteomic Analysis of Cortical Regions of 5x-FAD Female Mice*

Unbiased quantitative proteomics identified 6724 proteins in cortical lysates, of which 164 were significantly increased and 262 were significantly decreased in *5x-FAD* compared to age-matched WT littermates, as shown in the heat map in **Figure 2**. Upregulated and downregulated proteins are listed in **Table 1** and **Table 2**, respectively (See Appendix A). Notable proteins known to increase during AD pathogenesis in models and humans were found in the upregulated group of brain lysates including AβPP, apolipoprotein E (APOE), clusterin, and glial fibrillary acidic protein (GFAP) lending validity to our proteomic results [12, 41, 50]. DAVID Gene Ontology (GO) function was used to analyze our list of significantly upregulated proteins separate from those that were downregulated allowing for distinctions of which pathways were enriched by these expression changes. Biological processes, cellular components, and molecular functions for each group were considered (**Figure 3A-C**). Numerous upregulated proteins in our AD model were strongly associated with facilitating synaptic communication, particularly glutamatergic signaling, with both ionotropic (NMDE2) and (GRM1) metabotropic mechanisms being enriched.

In regards to analyses of biological processes, regulatory proteins involved in clearance of amyloid plaques had the highest fold enrichment amongst the upregulated proteins. Several mitochondrial metabolic proteins (ATPA) were downregulated, which has been well documented in the context of AD in both models and humans [40, 42]. In addition, proteins involved in the development and maintenance of the cytoskeleton and inhibiting depolymerization and transportation along actin filaments were decreased.

Cellular components results were associated to the cytosol, glutamatergic synapses and postsynaptic membranes supporting the idea that synaptic changes could be a crucial factor at this stage in AD. Proteins that contribute to forming the cytoskeleton and the major components of the myelin sheath had the most conserved decrease amongst the groups. Although proteins important for maintenance of the myelin sheath have been observed to be disrupted in AD, further characterization of these proteins could contribute to understanding myelin's role in this disease's pathogenesis [20, 51, 52]. Interestingly, an enrichment of downregulated proteins related to glutamatergic synapses was also observed which agrees with results found in humans from other

groups. Molecular function analysis revealed enrichment in ATP binding, dehydrogenase, and oxidoreductase activity.

### *Secondary Validation of Protein Targets of Interest from the Bulk Proteome*

Protein targets of interest were selected by reviewing raw proteomic data for consistent changes in expression across all samples from both control and transgenic groups. Western blot analysis was utilized for validation of protein expression changes found in our proteomics data from *5x-FAD*. GFAP and myelin oligodendrocyte associated basic protein (MOBP) were representative targets for upregulated and downregulated protein from our whole proteome group, respectively, as they have been established to have expression changes in human AD progression [20, 40]. Quantitative analysis using ImageJ software was performed on Western blot images (**Supplemental Figures 3-8**) and is displayed in **Figure 4A-C** (n=5-8 per group. *p*-value displayed). GFAP expression was confirmed to be upregulated in *5x-FAD*, whereas MOBP showed no significant change between groups. S-nitrosylated MYPR was decreased in *5x-FAD* compared to WT littermates. To ensure that the biotin switch method did not exert an effect on S-nitrosylated results, sample without reducing and labeling reagent underwent affinity purification and Western blotting to confirm that there was not a difference between overall MYPR expression (**Figure 4D**).

### *S-Nitrosylated Proteome in Cortical Lysates of 5x-FAD*

Following affinity purification through the biotin switch method, samples underwent mass spectrometry. Results identified 61 proteins with significantly increased levels of S-nitrosylation and 164 with significantly decreased S-nitrosylation which are collectively displayed in **Figure 5** through a heat map with corresponding cluster profile plots. These data were also categorized using DAVID GO database and at least 6 of the top 10 groups from biological processes, cellular components, and molecular functions results shared a combination of amyloid-beta precursor protein (A4), apolipoprotein E (APOE), apolipoprotein A-I (APOA1), which are related to the development of FAD (**Supplemental Figure 1A**). Proteins with decreased S-nitrosylation were associated with an enrichment of metabolic processes within the mitochondria affecting both inner and outer membranes. (**Figure 6A-B** and **Supplemental Figure 1B**). Interestingly, there was a

conserved decrease of S-nitrosylation in six tRNA protein ligases whose expression levels were not decreased in analysis of the whole proteome (**Figure 6C** and **Supplemental Figure 1C**). Similar to the bulk proteome, 24 proteins contributing to myelin sheath formation and maintenance were downregulated, supporting the idea that dysregulation of these proteins could be linked to the progression of AD (**Figure 6B** and **Supplemental Figure 1B**). Molecular function annotation also revealed decreases in S-nitrosylation of 6 potassium channels, whose role in AD are not completely understood, as well as proteins involved with oxidoreductase activity (**Figure 6C**). There were 12 proteins with increases in expression that also showed increased S-nitrosylation, including, AβPP, APOE, clusterin and GFAP. Twenty-six (26) proteins showed decreased expression levels across the whole proteome along with decreases in S-nitrosylation.

Myelin proteolipid protein (MYPR) demonstrated a conserved decrease across *5x-FAD* samples compared to WT littermates with a $\log_2$ fold change of 1.72, therefore we chose this protein to represent our S-nitrosylated data. To ensure that the biotin switch method did not exert an effect on S-nitrosylated results, sample without reducing and labeling reagent underwent affinity purification and Western blotting to confirm that there was not a difference between overall MYPR expression (**Figure 4D**).

***Phosphoproteome and Acetylome Alterations***

Detection of differential phosphorylation and acetylation within the cortex of our AD model was carried out by Progenesis QI software: 3,024 phosphopeptides had been identified, and those with a *p*-value higher than 0.05 as assessed using a One-Way ANOVA were removed from the dataset. As a result, 161 peptides from 90 different proteins showed significantly altered phosphorylation levels with one, two, three, or four unique phosphorylation sites. GO annotations were assessed for phosphopeptides and results with less than 1% false discovery rate (FDR) were represented as nodes in **Figure 7**. Molecular functions of phosphopeptides identified within our data set concur with current studies that state differential phosphorylation of proteins involved in cytoskeletal, protein kinases, and heat shock proteins are observed in AD progression in humans [38, 53]. Four major protein:protein interaction networks were established with high confidence using STRING analysis. One network with the highest confidence functioned in recruitment dynamics of endocytosis and exocytosis with Myc box-dependent-interacting protein 1 linking the

network to APP. The network with the next highest confidence was related to neuron morphology and axon myelination. Interestingly, three isoforms of the alpha subunit of sodium/potassium-transporting ATPase showed increases in phosphorylation while one isoform of the beta subunit showed decreases. This network is represented on the map but is not known to interact with APP (**Figure 8**).

Analysis of 538 acetylated peptides resulted in 24 peptides with significantly affected acetylation modifications. These 24 peptides belonged to 20 unique proteins with two proteins displaying two acetylation sites. A volcano plot was used to visualize proteins whose acetylation levels were the most significantly affected (**Supplemental Figure 2**). Dihydropyrimidinase-related protein 2 (DPYL2) and Histone H2B type 2-B (H2B2B) showed the largest decrease and increase in acetylation levels, respectively. Histone acetylation has been reported to have a role in the etiology of AD as well as age related cognitive impairment [54]. A protein:protein network of our acetylated proteins in **Figure 8** shows a node of three different histones known to interact at a high confidence level. It has been reported that histone acetylation is important in cognitive function and deregulation of genetic material could play a role in decreases in learning and memory [55]. We also observed decreased acetylation of three subunits of mitochondrial protein ATP synthase.

## Discussion

Investigation into the molecular pathogenesis of Alzheimer's disease in humans has provided the research field with pathogenic factors such as Aβ and tau [9]. These proteins have been utilized to create transgenic murine models to replicate critical aspects of the disease; however, no one mouse model has been able to fully recapitulate human AD, particularly those of sporadic nature, which are the vast majority of AD cases. Although limiting, investigation of each could lend itself to the benefit of understanding causal or consequential protein changes to certain areas of the brain and how they compare to humans. Our study was purposed to investigate these protein alterations in expression and post-translational modifications to elucidate broad biological pathways and novel proteins of interest.

Proteins with an observed increase in expression from the bulk proteome shared a common biological process of conduction of synaptic transmission at glutamatergic synapses through metabotropic and ionotropic receptors. This was well represented in GO analysis of the proteins' cellular component as the proteins in the increased population were strongly associated to glutamatergic synapses with only a five-protein difference between the groups with the strongest enrichment. Glutamate signaling within the synapse has been shown to participate in the formation of long-term synaptic plasticity connections and promoting neuron survival [32]. However, extrasynaptic glutamate signaling is contraindicative of beneficial pathways and can have compounding effects of neurodegeneration in AD [32]. Enrichment of proteins associated to excitatory signaling also supports the suspected role that excitotoxicity has in the development of AD and other neurodegenerative conditions through promotion of an oxidative environment [32, 33, 56].

Interestingly, our GO results for cellular components of proteins with decreased expression also highlighted a group associated with glutamatergic synapses as well. This is consistent with results found within human samples [40]. Increases in proteins present in glutamatergic synapses, although contradictory to human results, could be an early neuroplasticity response to overcome the known neurodegeneration in the model as consequence of Aβ plaques deposition. Additionally, several proteins were localized to the mitochondria and were involved with glyceraldehyde-3-phosphate dehydrogenase, whose enzymatic activity has been previously described to be decreased in AD patients, and oxidoreductase activity [57, 58]. Dysfunction of mitochondrial oxidoreductase

activity is strongly believed to be an additional source of ROS/RNS production in the onset of AD [59]. ROS are produced from the mitochondria at low levels and antioxidants can efficiently neutralize these molecules before they can alter protein function, but Aβ species can interact with mitochondrial macromolecules leading to increases in oxidative stress and apoptosis [59, 60]. Our results also highlight a decrease in proteins associated with cell morphology specifically maintaining the polarity of neurons as well as the myelin sheath. Decreases in cytoskeletal proteins could be representative of a neuron atrophy and synaptic loss associated with Aβ plaque deposition in regions of the brain that are myelinated later in development [52]. Myelin damage has been documented in humans with AD and in *5x-FAD*, but it is often associated with being an effect of neurodegeneration [51, 61]. Recent studies have challenged this dogma, and new data support the possibility that AD pathogenesis could be linked to early oligodendrocyte damage and may precede neuronal degeneration [52, 61]. Additionally, specific proteins that contribute to forming the myelin sheath including MOBP, myelin-oligodendrocyte glycoprotein (MOG), and myelin-associated glycoprotein (MAG) were among the top ten most effected proteins within our decreased dataset and have also been found to be altered in AD patients and some other mouse models [51].

To validate our proteomic data and confirm that our findings are consistent with other laboratories, GFAP was chosen as a representative upregulated protein for Western blotting. GFAP is an intermediate filament-III protein exclusively expressed by astrocytes in the central nervous system responsible for cytoskeleton structure and strength. Expression is increased in response to brain injury and chronic overexpression is regarded as having negative impacts on physiological recovery mechanisms [62].Recently, findings have correlated circulating GFAP levels with severity of brain injury and multiple sclerosis, increasing the clinical potential of GFAP as a biomarker for AD [63].We observed an increase in GFAP expression in *5x-FAD* brains, similar to what was reported AD, Parkinson's disease, and traumatic brain injury patients [40, 62]. An observed novel, upregulated protein within our data was hydroxypyruvate isomerase (HYI). This protein has the highest significance amongst increased proteins and the highest fold-change. HYI catalyzes the isomerization between hydroxypyruvate and 2-hydroxy-3-oxopropanoate. Little is known about this protein, but its expression has also been shown to be increased when the alpha-2 isoform of the AMPK catalytic subunit is removed from aging mice. These mice demonstrated impairment of long-term object recognition memory compared to AMPK alpha-$1^{-/-}$ whose abilities

were improved in this area [64]. Increases in this protein could be a consequence of dysregulated AMPK signaling in normal aging and could have a role in memory loss [64]. In the context of AD, investigation of this protein is minimal, but further efforts could elucidate potential pathological effects of overexpression of HYI. Our representative downregulated protein for Western Blotting analysis was MOBP as it has been shown in at least one study to be upregulated in hippocampi of *5x-FAD* mice at a comparable age to those in our study [50]. MOBP is a form of a myelin basic protein (MBP) and is thought to have a role in stabilization of the myelin sheath [65]. Decreases in MOBP, MAG, and MOG could support the idea that these proteins could be more susceptible to damaging effects of early AD progression compared to proteolipid proteins that contribute to the myelin sheath that were found to be unaffected at this stage in the disease. Although decreases in MOBP, MAG, and MOG have been found in humans with AD and other AD models, differential expression patterns have not been definitively stated as being consequential or casual [51, 52, 61]. We observed no change in MOBP expression in the *5x-FAD* model following Western Blot quantification; however, a batch effect was evident and could be affecting the ability to draw accurate conclusions. Further studies could aim to document myelin sheath dysregulation in human AD pathology as well as clarify if the *5x-FAD* model parallels myelin injury progression.

S-nitrosylation has been known to be a redox-based post-translational modification that can increase in prevalence in the presence of higher production of nitrosative stress [43]. Although levels have been found to be abnormal in AD progression, understanding consequential effects depends on the target protein. GO annotations generated from proteomics data following affinity purification of S-nitrosylated proteins implicated the mitochondria along with the respiratory transport chain as being primary target of S-nitrosylation. Over the last decade, different studies showed that S-nitrosylation of mitochondrial protein dynamin-related protein 1, cyclin dependent kinase 5, voltage-dependent anion channels, and superoxide dismutase 2 could lead to increased mitochondrial fission and synaptic loss, dysregulated membrane permeability, and altered antioxidant defenses, respectively, in neurodegenerative diseases [43, 66-68]. Additionally, tricarboxylic acid (TCA) cycle enzymes such as alpha-ketoglutarate dehydrogenase, also found in our proteomic analysis, have been gaining interest in recent years for their AD pathogenic effects due to S-nitrosylation [69]. However, it has been suggested that this PTM could have benefits specifically at complex I of the electron transport chain. One group stated that S-nitrosylation mediated inhibition of complex I, through unknown mechanisms, could cause decreased ROS

production compared to inhibition of complex III [27]. Seven proteins associated to complex I biogenesis were found to be decreased in our S-nitrosylated data, with only one protein showing decreased expression, supporting the idea that differential modification of several subunits could contribute to reported inhibition.

Biological processes and molecular function analysis revealed an enrichment of translational enzymes and ribosomal structure proteins. Studies within the last five years have begun to show that tRNA molecules and tRNA synthetases (aaRSs) are modified and alterations in these modifications can have detrimental effects to translation or be adaptations to environmental stressors, especially those due to a high nitrosative environment [70-72]. aaRSs are ubiquitously expressed in the body and responsible for accurately attaching specific amino acids to respective tRNA molecules in the process of decoding mRNA [70]. These enzymes are localized to either the cytoplasm or the mitochondria. One study showed that decreases in S-nitrosylation of mitochondrial threonine tRNA synthetase led to decreases in aminoacylation in humans [43]. Decreases in S-nitrosylation of seven different aaRSs involved with cysteine, threonine, serine, histidine, aspartate, valine, and isoleucine were observed in our data. Six of these enzymes showed no differences in overall protein expression levels when compared to results from the whole proteome, despite their altered S-nitrosylation status. Literature concerning aaRSs role in health and disease is still scarce; however, there is evidence of an association between changes in tRNA and aaRSs PTMs with mitochondrial dysfunction and neurological disorders such as Huntington's disease [43, 71]. Exploring discrepancies in S-nitrosylation of aaRSs in the context of AD could be beneficial in understanding cellular stress responses that could be neuroprotective versus neurodegenerative.

An interesting result from cellular component analysis was the high confidence grouping of proteins involved in producing and maintaining the myelin sheath. Of the twenty-four proteins identified, four were directly related to myelin sheath structure and all showed decreases in S-nitrosylation. Only one protein, MYPR, showed no change in overall protein expression when cross referenced with decreased proteins from the whole proteome. MYPR functions in the formation and maintenance of the multilamellar structure of myelin and it constitutes 38% of total protein mass in the central nervous system [65]. Our data showed no differential expression levels of MYPR at the whole proteome level, and this is contradicted by one study done in 5x-FAD at

four months of age that observed increased expression in the hippocampus [41]. Tissue location and sex of the mice, which was not stated in this study, could contribute to the discrepancies in data as our results were exclusively made from females. One study incubated optic nerves from Sprague-Dawley rats with NO-donors which resulted in myelin decompaction and S-nitrosylation of MYPR [73]. Additionally, literature reporting on inflammatory neurodegenerative conditions such as multiple sclerosis states that ROS and RNS can overwhelm antioxidant defenses within oligodendrocytes contributing to demyelination [74]. Although evidence supports demyelination in AD, few studies have looked at whether a loss of expression or a change in modification is present at the most abundant myelin protein. Due to this, as well as the strong clustering in our proteomic data, we looked to quantify the amount of S-nitrosylated MYPR compared to controls. Western blotting analysis showed a decrease in S-nitrosylated MYPR in the cortex of 6-month-old female mice suggesting that S-nitrosylation of MYPR could be necessary for the functioning or folding of the protein. Our data could provide support for specific myelin protein structure changes that lead to anatomical changes in AD, however, additional efforts are necessary to clarify the nature of S-nitrosylated MYPR.

Two biomarkers that are utilized in diagnosing AD are Aβ plaques and hyperphosphorylated tau [9, 29, 36]. Increased phosphorylation of microtubule-associated protein tau and kinases or phosphatases responsible for the modifications have been well characterized by AD literature [10, 38, 53]. The *5x-FAD* mouse model expresses tau proteins and six phosphopeptides of this protein were differentially phosphorylated within our proteomic analysis; however, all sites showed increased phosphorylation in WT littermates. Although not used to study neurofibrillary tangles occurring in AD, the *5x-FAD* model could be valuable in uncovering differential phosphorylation of proteins by dysregulation of kinases and phosphatases apart from tau. GO results of identified phosphopeptides primarily implicated enrichment of pathways associated to microtubule dynamics. Microtubule and tubulin proteins have been shown to be phosphorylated in AD, but little is known about the functional effects this PTM has on such proteins [38, 75]. Our findings show increased phosphorylation of MAP2, MAP1B, and α-tubulin. Increased MAP2 phosphorylation has been suggested to promote axonal outgrowth while decreases in the MAP1B/P-MAP1B ratio has been found to decrease microtubule stability [76, 77]. Phosphorylation of α-tubulin is mediated through PKC-α activity and has been shown to cause increased cytoskeleton dynamics in human breast cells [75]. Although α-tubulin phosphorylation

is largely unstudied in AD, it is known that PKC-α acitivity is increased in the brain of AD patients, and similar effects could be taking place in *5x-FAD* [78]. Future studies focused on elucidating functional consequences of phosphorylation to microtubule proteins could lead to a better understanding of cellular responses to neurodegeneration.

Additionally, gene ontology annotations grouped phophospeptides of the sodium/potassium ATPase subunits into many categories. The Na,K-ATPase is fundamental in regulating ion homeostasis across all tissues in the body and is made up of α and β subunits. Alpha and beta subunits 1-3 are expressed in the brain, and can be cell specific. Alpha subunits are responsible for hydrolyzing ATP and binding $Na^+$ and $K^+$ ions. Beta subunits are necessary for the proper incorporation of the protein into cell membranes [79, 80]. Deficiencies in Na,K-ATPase α-subunit genes are associated with learning and memory impairments and these genes have been found to be changed in human AD brains [81]. Others have also observed decreases in total protein expression in murine astrocytes incubated with Aβ. Our results do not show a decrease in expression of total Na,K-ATPase; however, differential phosphorylation of α-subunits exist. *In vitro* studies have shown that phosphorylation of Na,K-ATPase can cause decreased activity of the enzyme [82]. Taken together, increased phosphorylation of Na,K-ATPase could be an event that precedes decreased expression of the protein contributing to cellular ion imbalances found in AD.

Evidence of acetylation modifications in AD have been growing and differential acetylation of histones have been the target of recent therapeutics for the disease [54]. Histones are proteins that form octamers within chromatin to regulate gene transcription by limiting transcription factor accessibility to the strands [54]. Strict mediation of histone acetylation and deacetylation underlies memory consolidation and dysregulation of this process is believed to have a role in age-related cognitive decline and AD. Four core histones exist and transient increases in acetylation of histones H2B, H3, and H4 are observed in mice during learning activities [55]. Our proteomic data show a decrease in acetylation of H2B type 1, but an increase in acetylated H2B type 2. These differences could be indicative of compensatory mechanisms occurring at an early stage of AD. Studies investigating the effects of differences in acetylation of histone subtypes are sparse, however, further identification of the brain acetylome in the context of AD would allow for findings on histone subtype acetylation patterns. Also, our findings reveal nine of twenty acetylated proteins are localized to the mitochondria with acetylation decreasing in seven. A recent study

reported on the first account of the human brain acetylome and found 85% of acetylated mitochondrial proteins decrease with AD [83]. Of note, our findings are in agreement with this report, as we also show conserved decreased acetylation of ATP synthase isoforms and subunits within the mitochondria. These data support the idea that acetylation of mitochondrial proteins could be a strong modulator of metabolic deficiencies known to occur in AD and further efforts should be made to functionally understand how these PTMs differ in normal physiological aging and AD progression.

**Limitations**

This study, although informative, does not capture the encompassing protein changes as samples were only collected from 6-month-old *5x-FAD* female mice. Other studies have reported on protein expression and differential protein modifications in AD with human and *5x-FAD* samples, however, sex differences have not been diligently investigated. This could lead to generalization of pathological stages and therefore, a lack of appreciation for physiological understanding. For example, our laboratory is currently uncovering potential mechanisms contributing to vasculature dysfunction in the *5x-FAD* that demonstrate differential PTM in females and altered intracellular $Ca^{2+}$ handling in males [84]. Biological females are twice as likely to develop AD compared to age-matched males and while AD etiology is not completely understood, potential sex differences should be acknowledged to support precision therapeutic treatments in the future. Our reported data highlights aspects of female disease progression, and therefore also lacks direct analysis between biological sexes. Further studies should look to address these details and meta-analyses could play a helpful role in organizing literary findings.

Additionally, this project captures proteome differences at only one stage of AD progression. Several studies mentioned here have detailed this gap in knowledge by looking at proteome changes ranging from one to twelve months of age in this same mouse model, but specific novelties reported in our data, primarily the brain acetylome, myelin sheath proteins, and aaRSs, are only beginning to be understood and require continued investigation.

Brain cortex homogenates were optimized to study S-nitrosylation levels through affinity purification to identify protein targets in an environment where molecules are at a high susceptibility to be modified. Due to this, remaining tissue was not adequate to undergo enrichment protocols to promote an ideal view of the phosphoproteome as well as the acetylome. Enrichment procedures to preserve phosphorylated proteins are prevalent and have yielded large, useful datasets; however, a comprehensive report on the human brain acetylome with changes during AD has been recently documented. As literature grows to deepen our knowledge of differential acetylation in AD, comparisons between *5x-FAD* and humans with AD should be made to assess the validity that the mouse model has in this emerging field. Furthermore, the biotin switch method is a common, although indirect method to enrich S-nitrosylated proteins and because of this,

further studies should look to verify our findings through more direct methods, such as SNOTRAP that not only enriches modified proteins but tags amino acid sites.

Lastly, as with other primarily omics-based reporting, the functional nature of how protein expression exerts its effects on disease is an aspect yet to be detailed for our results. Protein validation provides potential, preliminary candidates for cell culture experiments to understand if pathological characteristics can be replicated in a functional unit. Additionally, *in vitro* experiments will be foundational to study the effects that post-translational modifications have on specific protein functions in AD. These tests, along with further validations of results reported here, will clarify cellular mechanisms that contribute to AD progression.

## Conclusion

In this study, we utilized HPLC-ESI-MS/MS to identify proteome wide changes in protein expression and phosphorylation and acetylation peptides alterations. Additionally, we employed an affinity purification method to enrich S-nitrosylated proteins to ultimately validate proteins of interest, through Western blotting, alongside targets chosen from the whole proteome results. Our data demonstrates that numerous protein modifications take place in the stages leading to Aβ plaque saturation within the cortex, in conjunction with altered protein expression levels in *5x-FAD* females. Results concur with previously established protein expression changes existing in humans and animal models alike, while also addressing proteins groups through GO annotations that are novel to AD association. This is demonstrated by quantified increases in GFAP and decreases in MOBP expression as well as decreased levels of S-nitrosylated MYPR compared to age-matched WT controls through proteomic and Western blotting analysis. Decreases in S-nitrosylated MYPR could suggest that the modification could contribute to proper functioning or folding of the protein in normal physiology and alterations in such could have pathological effects. Additional proteins directly contributing to myelin sheath structure also showed decreases in S-nitrosylation including MOBP, MOG, and MAG. However, overall expression was decreased as well. Observed protein novelties include S-nitrosylation of aaRSs. Decreased S-nitrosylation of at least one aaRSs has been associated with increases in protein translation in neurological disorders, we report on six additional aaRS proteins existing in the cytosol and mitochondria with decreases in this modification that could contribute to Aβ-mediated translational dysregulation in AD. Furthermore, HYI upregulation could be an emerging target protein for memory impairment mechanisms as recent evidence of AMPK pathway pharmaceutical manipulation for AD therapeutics continues to be investigated. To conclude, our proteomic findings not only align with, but elaborate upon well-established protein changes, post-translational alterations, and enriched GO annotations found in humans suffering from AD and animal models implicating specific proteins involved in cytoskeletal organization, mitochondrial ATP genesis, ion homeostasis, transcription, translation, and myelin sheath maintenance contributing to characterization of the multifactorial nature of AD.

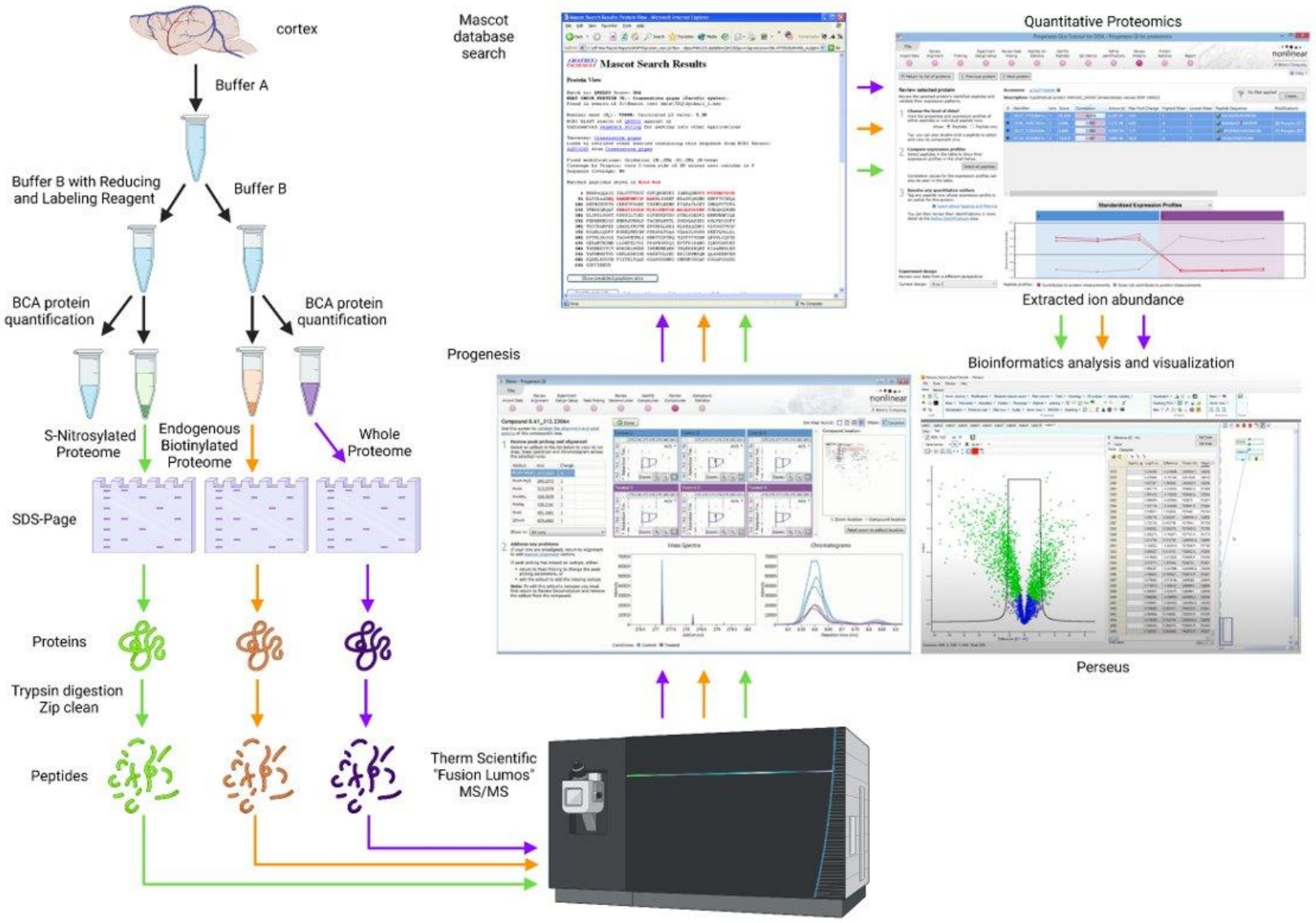


**Figure 1.** Sample Preparation Study Design. Brain cortex was taken from 6-month-old, female transgenic mice and age-matched controls. Homogenates were segregated to receive accurate representations of the Whole Proteome and S-Nitrosylated Proteome with the Endogenously Biotinylated Proteome serving as a control for the latter (n=3). Samples were subjected to gel separation, trypsin digestion, and tandem mass spectrometry followed by quantitative proteomics. Figure generated with BioRender.

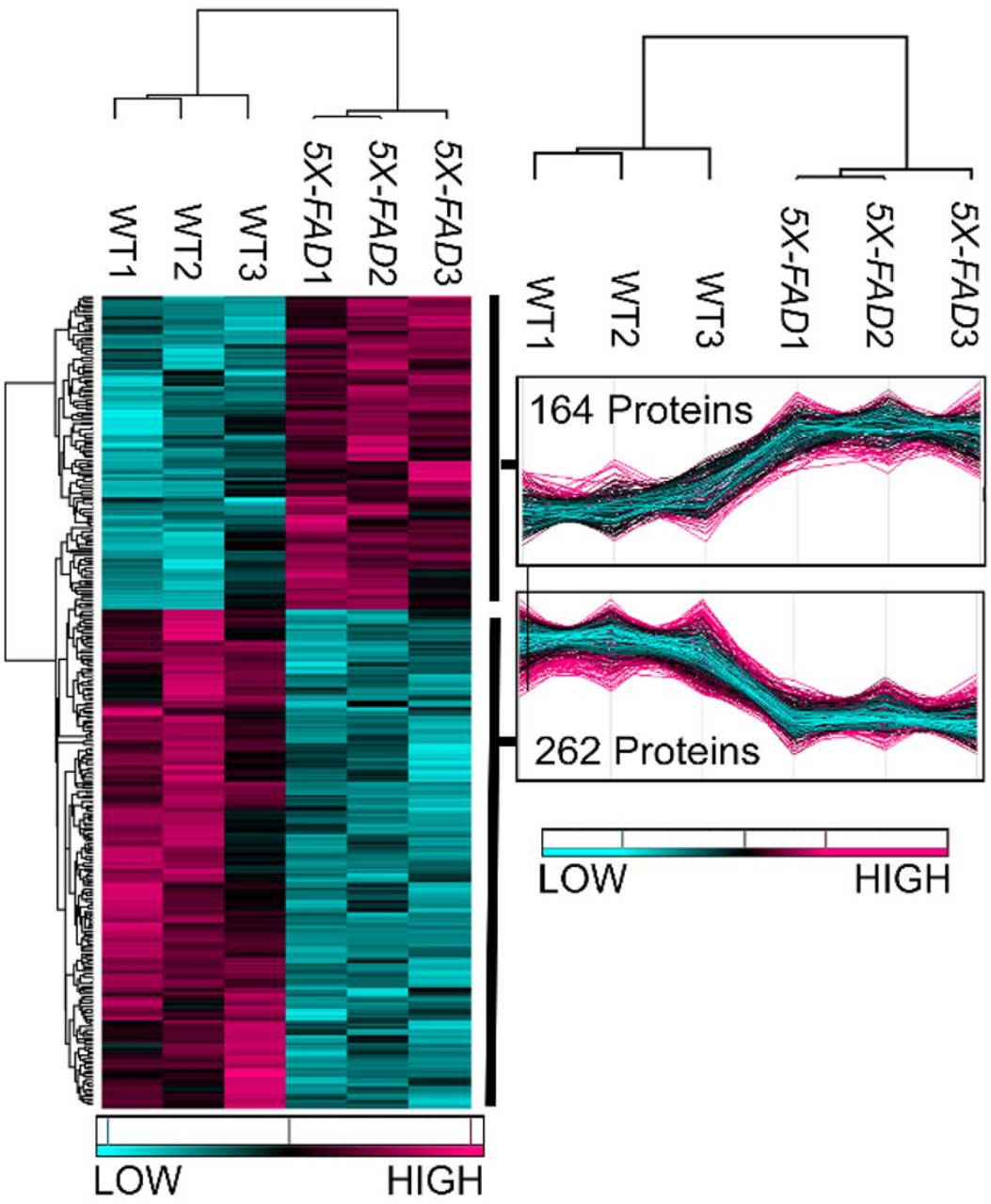


**Figure 2.** *Whole Proteome Protein Expression of 5x-FAD Females*. **A.** Heat mapping of individual protein expression levels from 426 significantly altered proteins demonstrating clear groupings between transgenic model and age matched controls (n=3, $p < 0.05$, One-way ANOVA). **B.** Protein abundance values underwent clustering analysis indicated by profile plots and show differential expression patterns between groups.

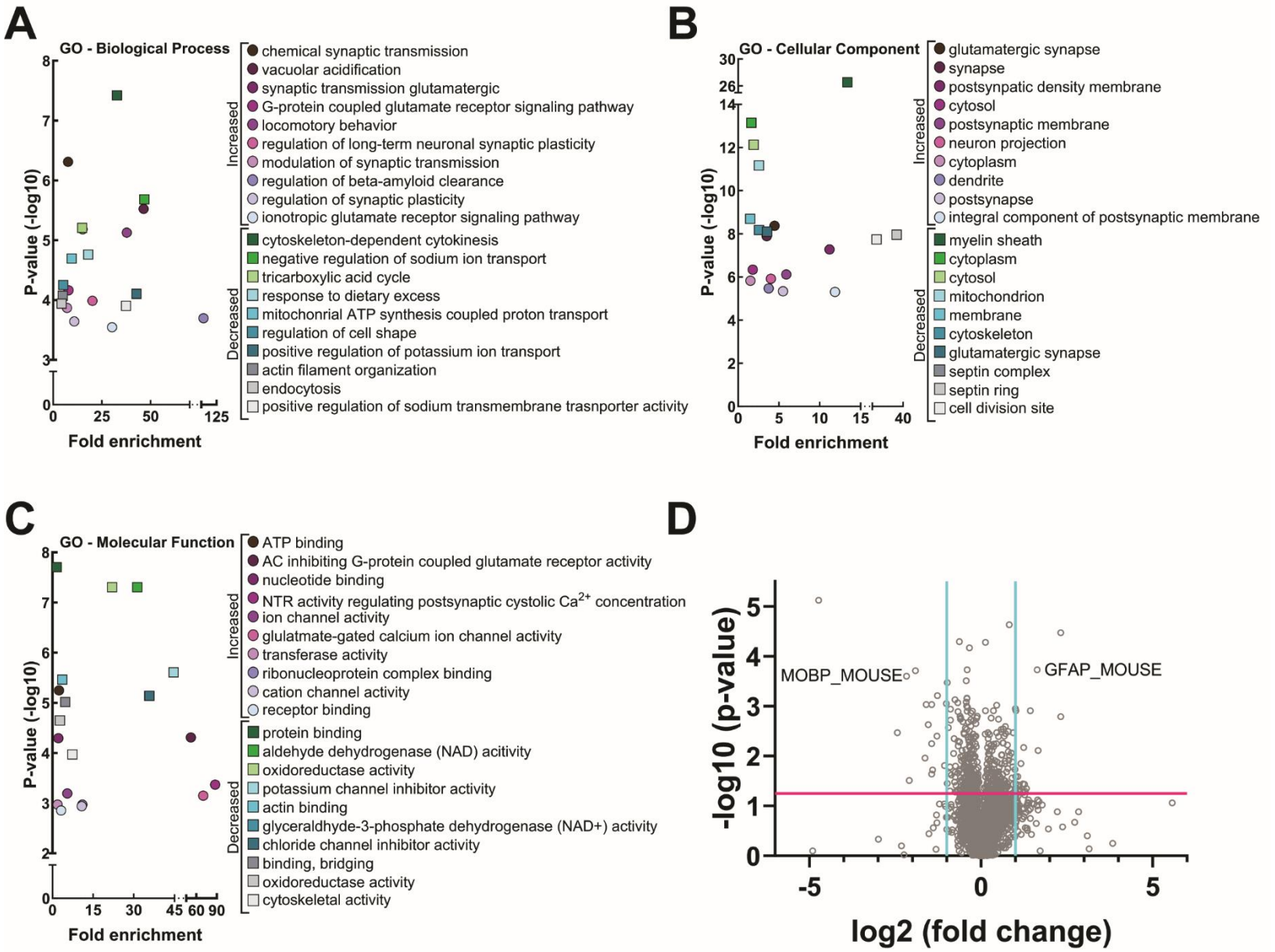


**Figure 3.** *Gene Ontology Enrichment of Altered Proteins* **A-C.** Top ten most enriched terms pertaining to biological processes, cellular components, and molecular functions, respectively, belonging to the increased and decreased proteins populations (FDR < 0.01). **D.** Volcano plot of differential protein expression in transgenic model. MOBP and GFAP are labeled as representative proteins of interests.

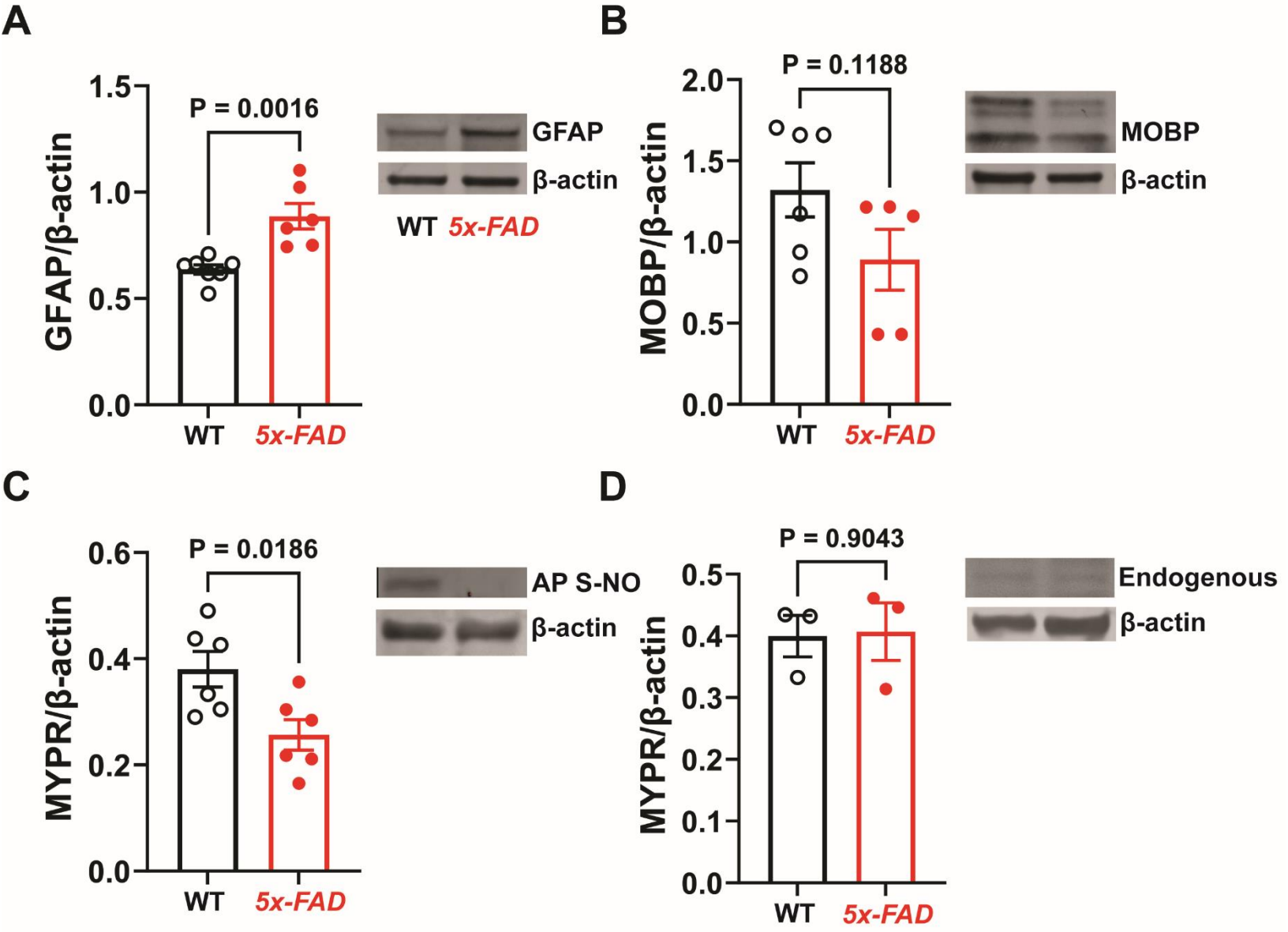


**Figure 4.** *Western Blot Quantification of Representative Proteins* **A.** GFAP was upregulated in brain cortex tissue. **B.** MOBP expression was unchanged compared to controls. **C.** MYPR S-nitrosylation was decreased in *5x-FAD* females following biotin switch and affinity purification. **D.** MYPR quantity without labeling reagent was unaffected following affinity purification (n=3-7), $p < 0.05$, Two-tailed t-test).

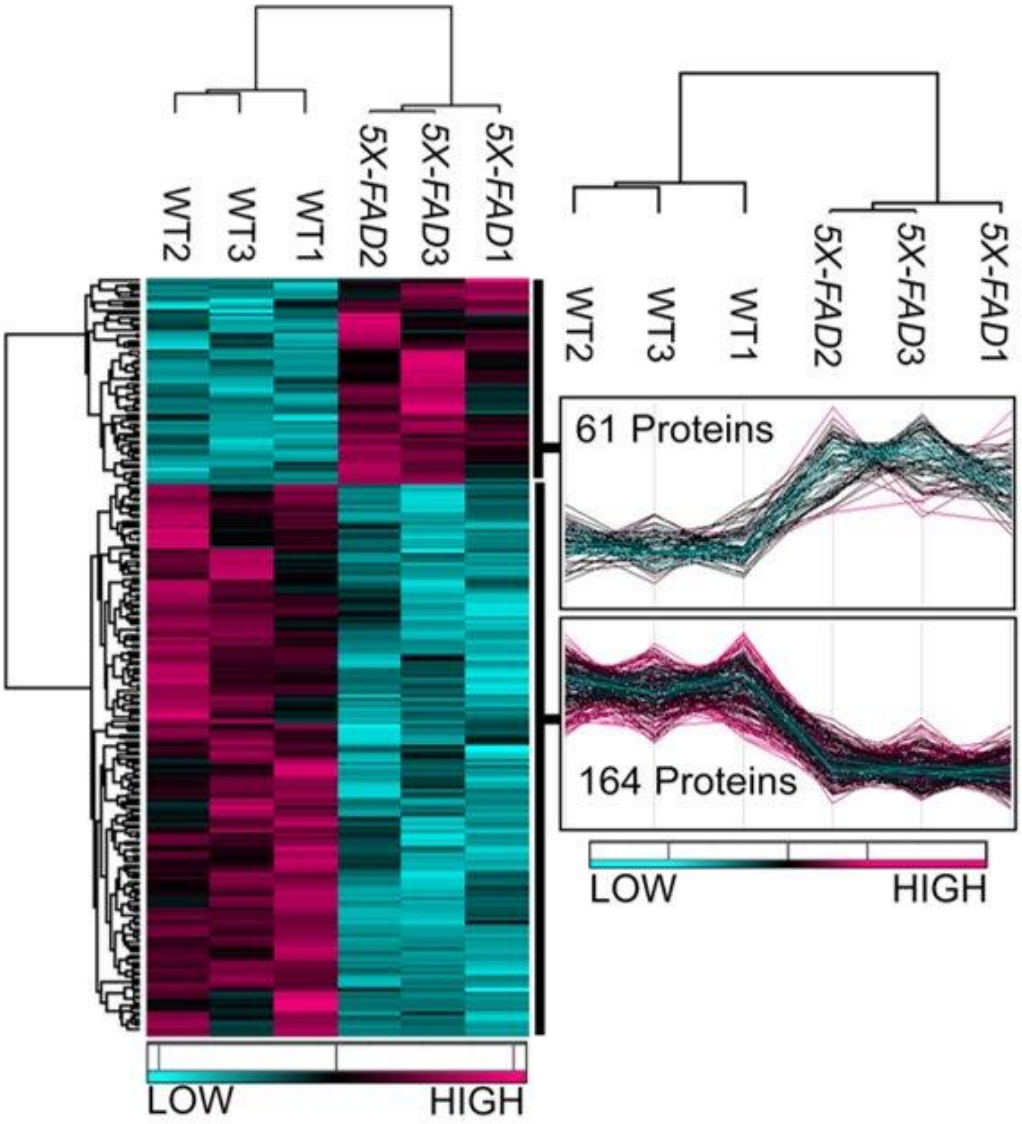


**Figure 5.** *Differential S-nitrosylation of Proteins* **A.** Hierarchal clustering of individual protein levels from 225 proteins showing differential levels of S-nitrosylation. Expression levels clustered after Z-score normalization (n=3, $p < 0.05$, One-way ANOVA). **B. N**ormalized protein abundance values underwent clustering analysis and show relative protein measurements using defined clusters for each indicator.

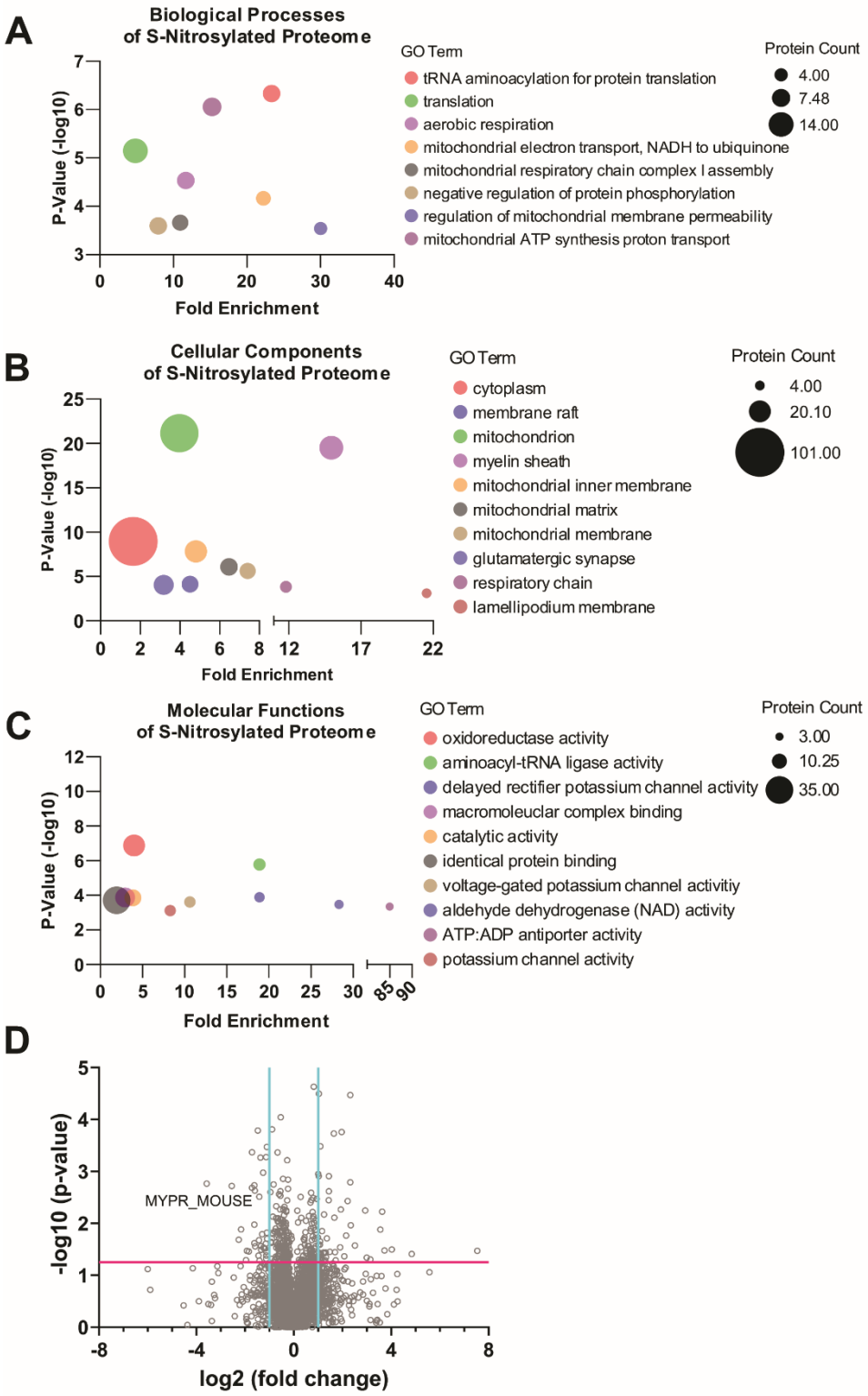


**Figure 6.** *Gene Ontology Annotation of Significantly Altered S-nitrosylated Protein* **A-C.** Most enriched canonical terms pertaining to biological processes, cellular components, and molecular functions, respectively, belonging to proteins groups with altered S-nitrosylation (FDR< 0.05). **D.** Volcano plot of differential S-nitrosylation made to individual proteins. MYPR is labeled as a representative protein of interest.

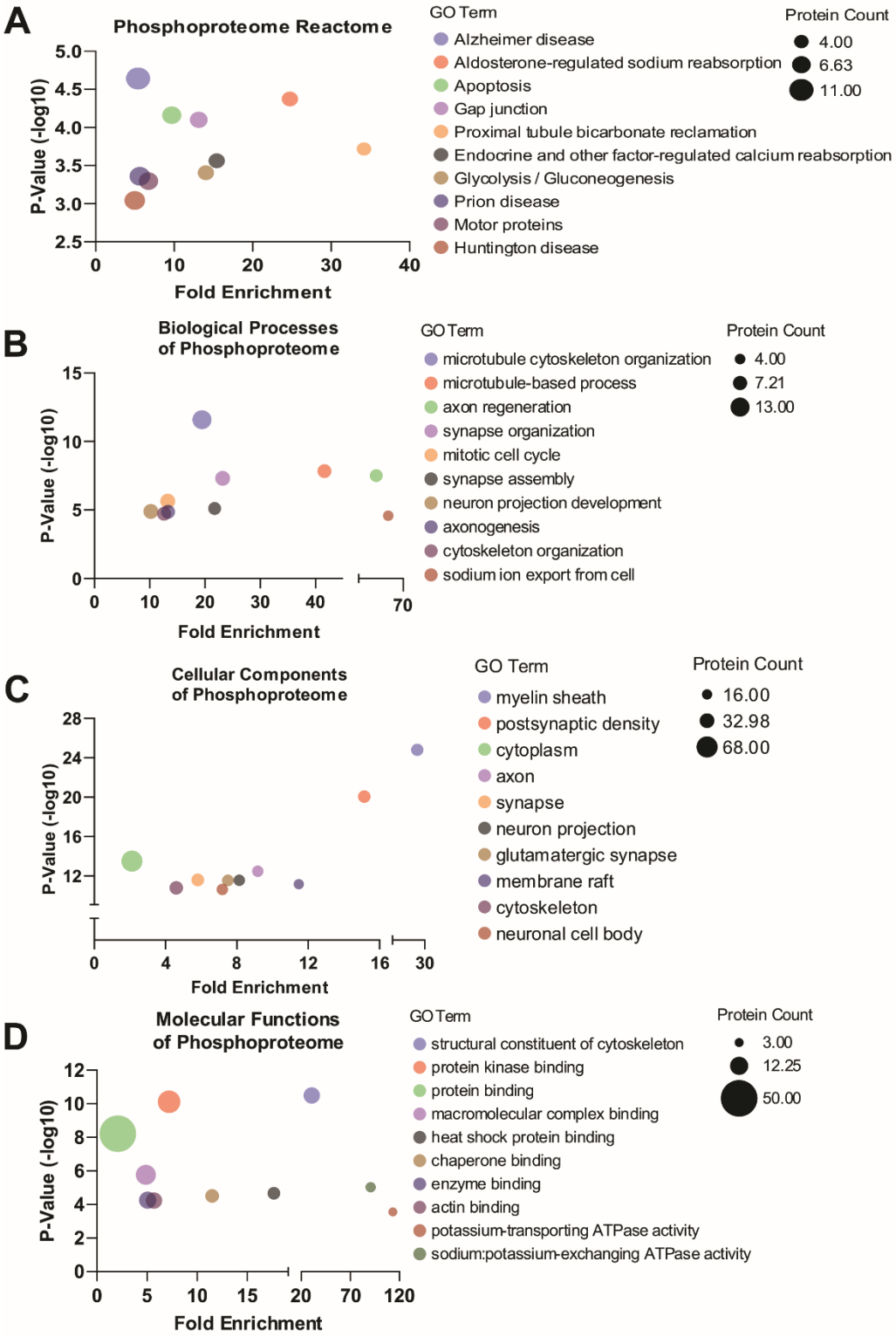


**Figure 7.** *Gene Enrichment Analysis of Phosphopeptides* **A-D.** Most significantly enriched results using peptides with differential phosphorylation patterns between groups (FDR < 0.01). Node size is representative of the number of phosphopeptides within respective groups.

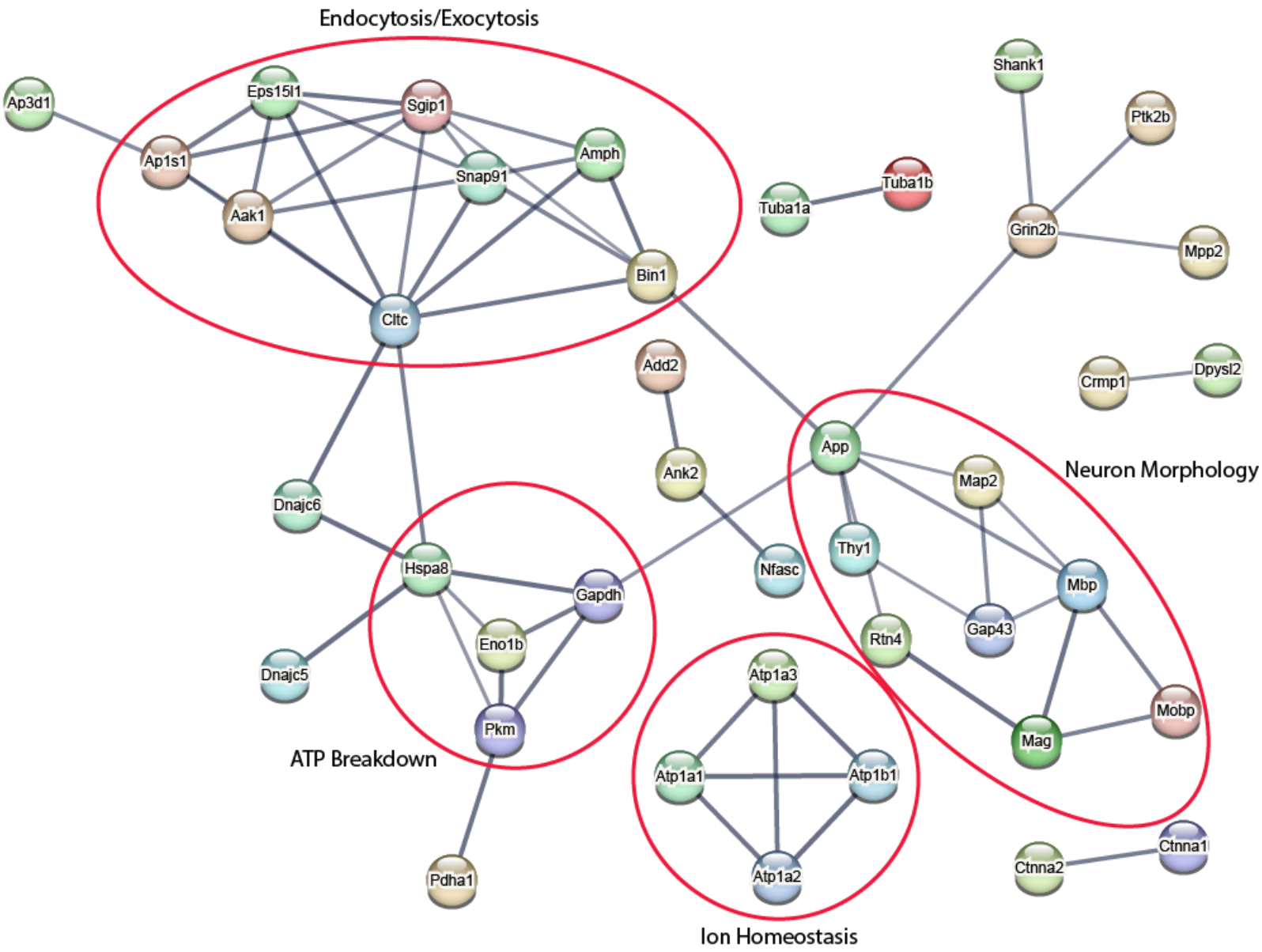


**Figure 8.** *Protein-Protein Interaction Network of Phosphopeptides* Edges indicate functional and physical protein interactions. Line thickness is indicative of the strength of supporting data. Network shows high confidence (score >0.7) associations.

## Supplemental Figures

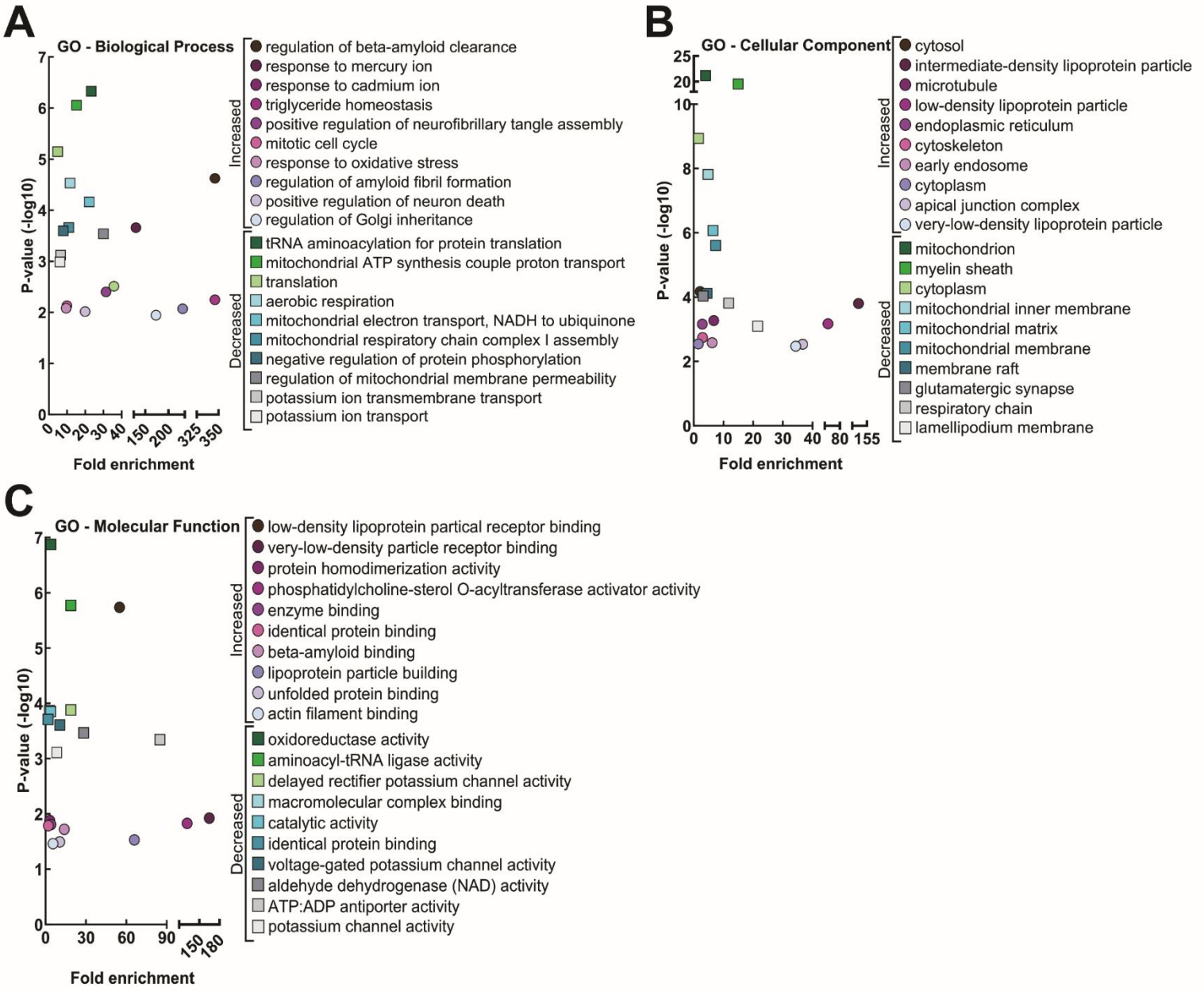


**Supplemental Figure 1.** *Gene Ontology Enrichment of Increased and Decreased Proteins* **A-C.** Top ten most enriched terms pertaining to biological processes, cellular components, and molecular functions, respectively, belonging to the increased and decreased proteins populations.

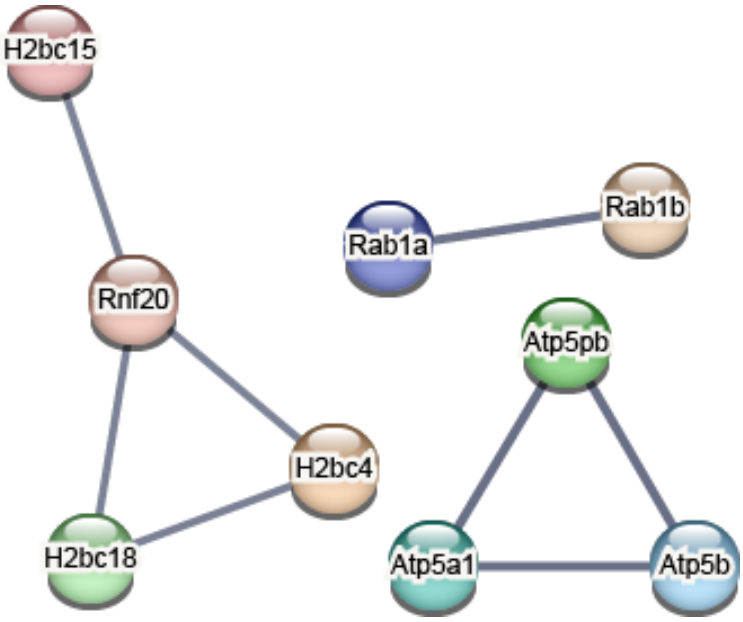


**Supplemental Figure 2.** *Differential Acetylome Protein-Protein Interaction Network* Protein-protein interaction network of peptides with significantly different acetylation levels. Edges indicate functional and physical protein interactions. Line thickness is indicative of the strength of supporting data. Network shows high confidence (score>0.7) associations.

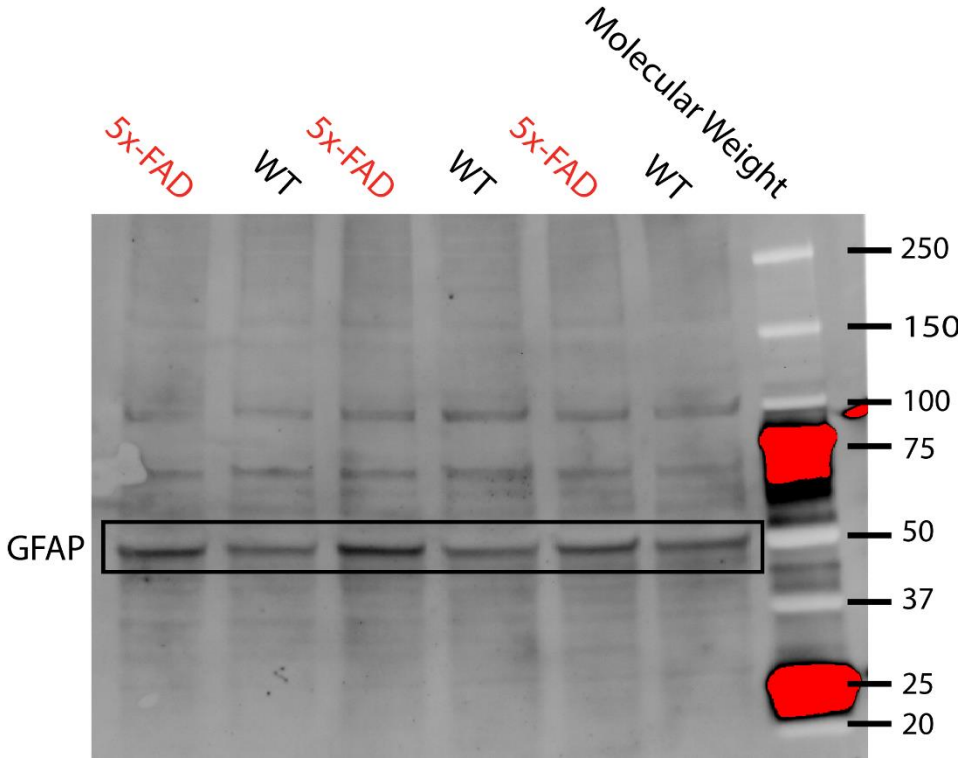


**Supplemental Figure 3.** *Representative blot of GFAP*

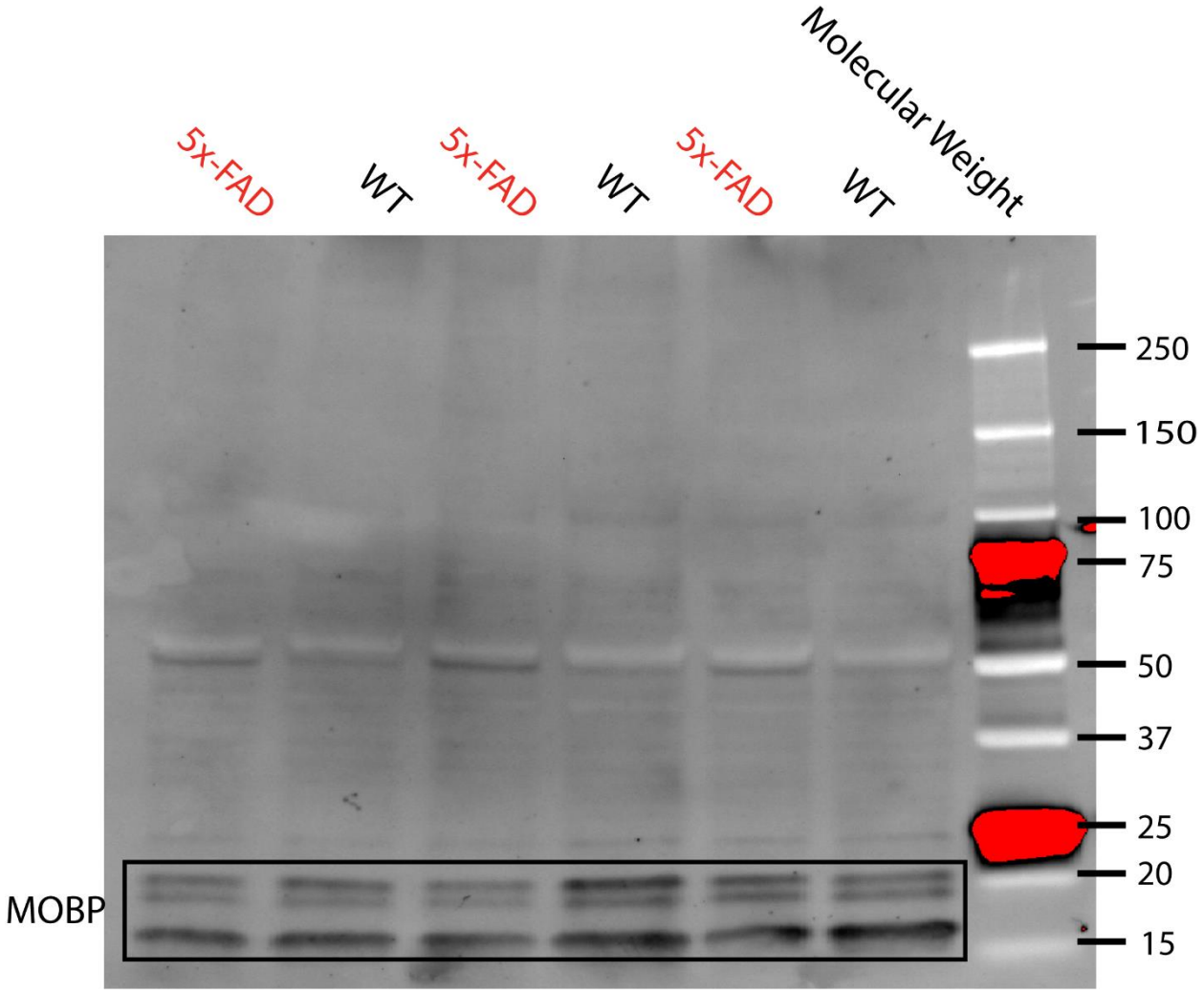


**Supplemental Figure 4.** *Representative blot of MOBP*

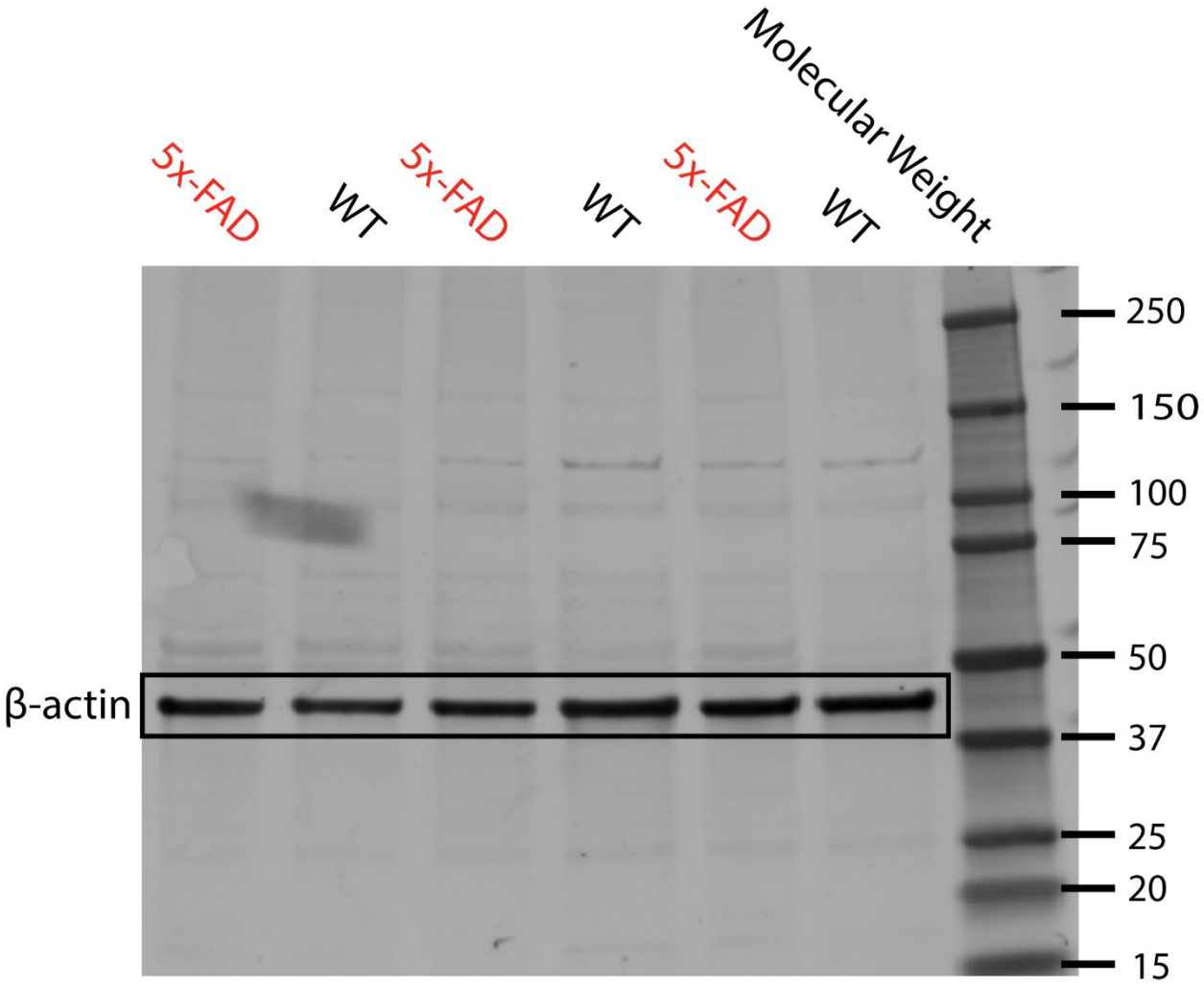


**Supplemental Figure 5.** *Representative blot of β-actin*

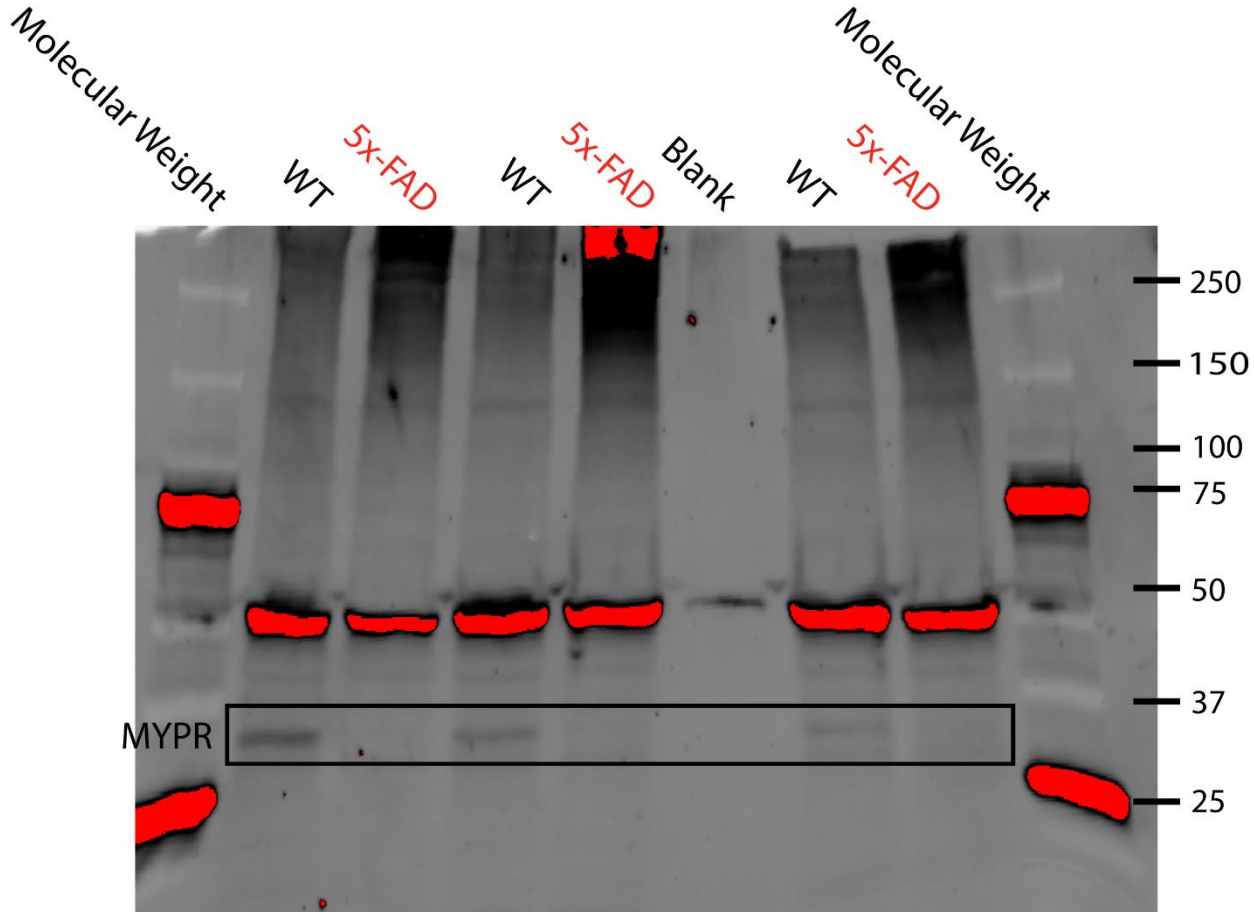


**Supplemental Figure 6.** *Representative blot of MYPR following SNO Affinity Purification*

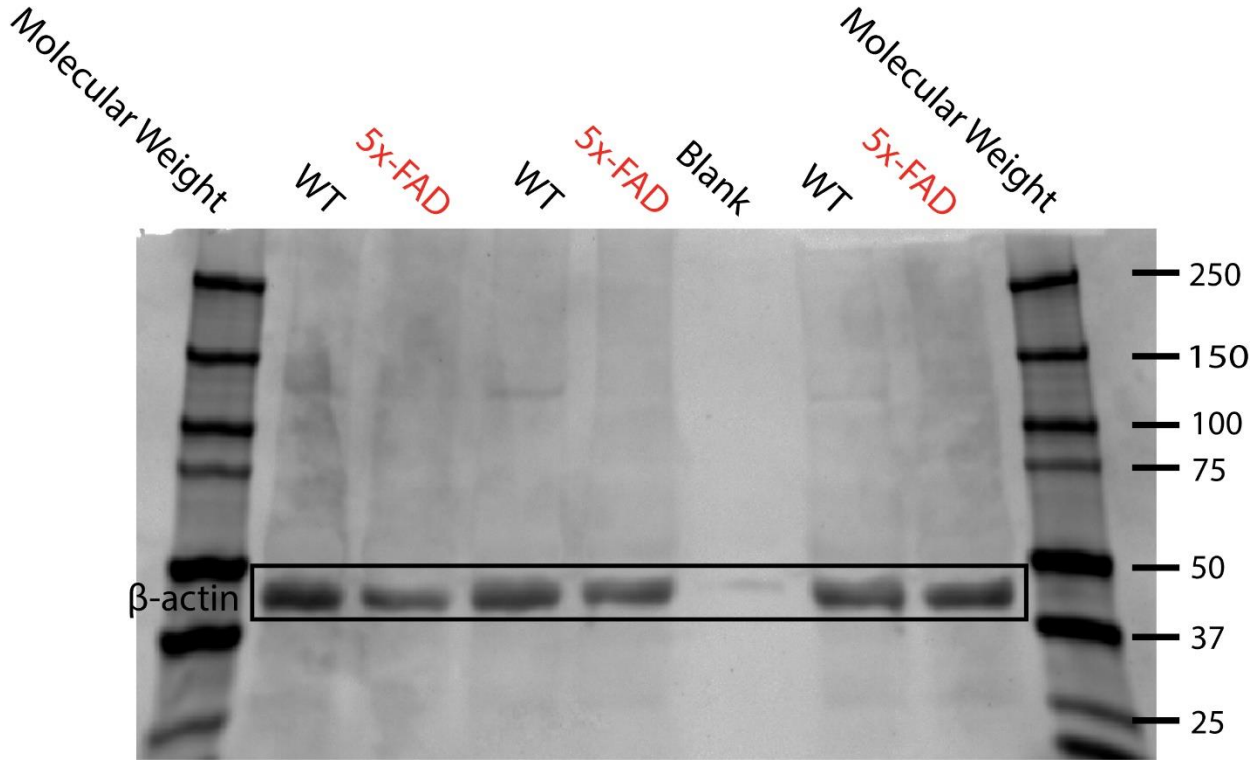


**Supplemental Figure 7.** *Representative blot of β-actin following SNO Affinity Purification.*

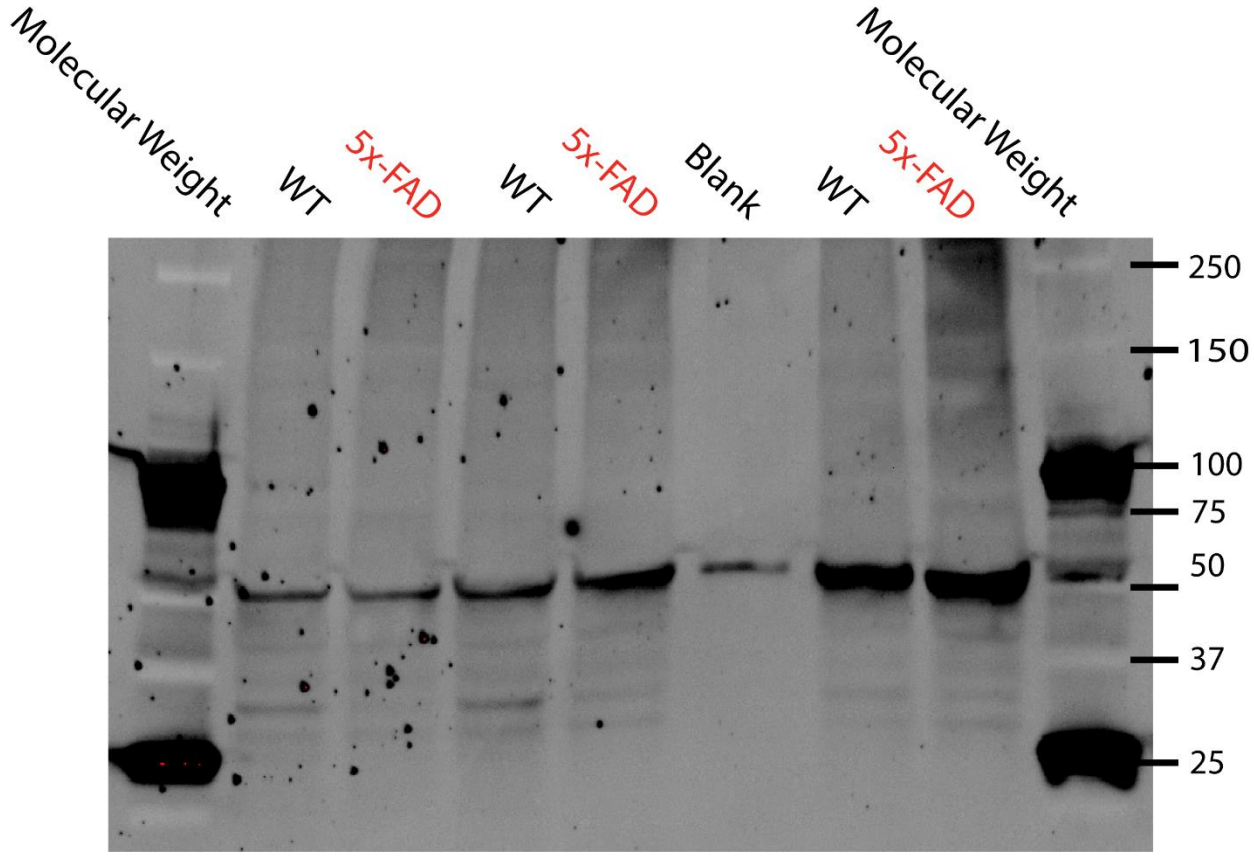


**Supplemental Figure 8.** *Representative Blot of MYPR from Control Sample Preparation*

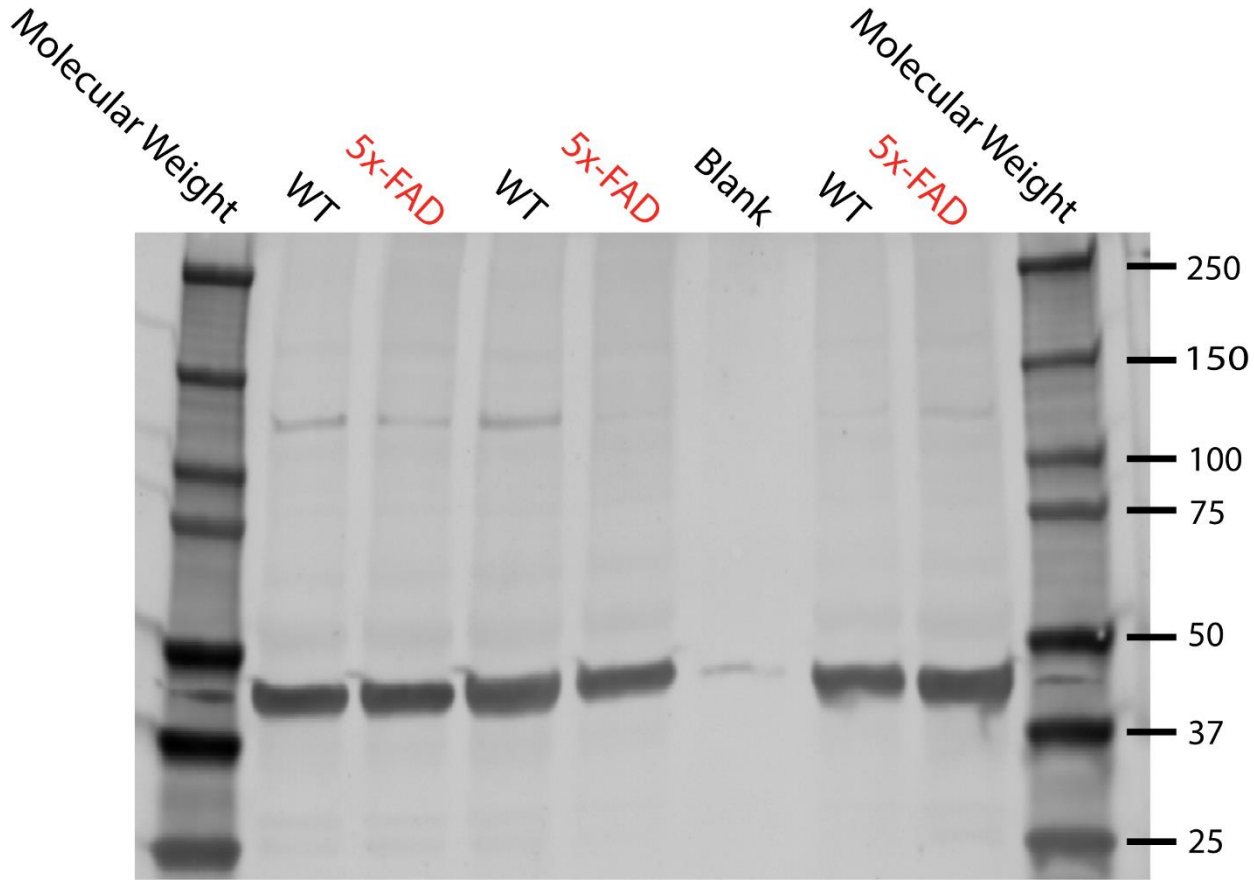


**Supplemental Figure 9.** *Representative Blot of β-actin from Control Sample Preparation*

## APPENDIX A

Table 1

Significantly upregulated proteins in brain cortex of *5x-FAD* female mice

| Gene Symbol | No. of unique peptides | $Log_2$ of fold change | $-Log_{10}$ of P-value | Gene Symbol | No. of unique peptides | $Log_2$ of fold change | $-Log_{10}$ of P-value |
|---|---|---|---|---|---|---|---|
| CO4B | 6 | 2.32 | 2.79 | WIPI3 | 2 | 0.52 | 1.35 |
| HYI | 3 | 2.32 | 4.47 | OSGEP | 9 | 0.52 | 1.63 |
| TM245 | 3 | 1.66 | 2.11 | PFD5 | 6 | 0.51 | 2.74 |
| GFAP | 36 | 1.64 | 3.73 | JPH4 | 3 | 0.51 | 2.39 |
| SGPL1 | 4 | 1.44 | 2.91 | DMXL2 | 127 | 0.51 | 1.49 |
| LEG3 | 2 | 1.32 | 1.35 | SERC1 | 2 | 0.50 | 1.43 |
| TM9S4 | 2 | 1.27 | 1.43 | PCD19 | 2 | 0.50 | 1.68 |
| UBR4 | 43 | 1.24 | 2.17 | GRM5 | 12 | 0.50 | 1.52 |
| STT3A | 3 | 1.22 | 1.44 | PDZ11 | 3 | 0.49 | 1.61 |
| MA2B1 | 2 | 1.16 | 1.85 | PAFA | 4 | 0.47 | 1.88 |
| CAC1E | 5 | 1.12 | 1.33 | DOC11 | 5 | 0.47 | 1.32 |
| KCND3 | 2 | 1.11 | 1.32 | ANM5 | 11 | 0.46 | 3.02 |
| HACD3 | 6 | 1.11 | 1.42 | ITM2B | 2 | 0.46 | 1.54 |
| TEN3 | 15 | 1.08 | 1.31 | CLUS | 13 | 0.46 | 2.47 |
| TM9S2 | 2 | 1.07 | 1.59 | SCG3 | 4 | 0.45 | 1.67 |
| MTND | 2 | 1.02 | 2.91 | PPIH | 2 | 0.45 | 2.25 |
| CAC1B | 9 | 1.02 | 1.44 | SCAM3 | 8 | 0.44 | 1.36 |
| P2Y12 | 2 | 1.01 | 1.59 | 3BP1 | 11 | 0.43 | 1.51 |
| RB33A | 4 | 1.01 | 1.37 | DMXL1 | 26 | 0.42 | 1.31 |
| A4 | 22 | 1.00 | 2.95 | RN112 | 2 | 0.41 | 1.67 |
| GPC5B | 6 | 0.99 | 1.73 | ZZEF1 | 22 | 0.40 | 1.91 |
| AGRB3 | 4 | 0.99 | 1.32 | PEAK1 | 8 | 0.39 | 1.73 |
| ATP9A | 5 | 0.94 | 1.43 | THG1 | 2 | 0.39 | 1.84 |
| NUDC1 | 3 | 0.94 | 2.47 | CPNS1 | 7 | 0.38 | 1.31 |
| SCN1A | 2 | 0.92 | 1.78 | SASH1 | 6 | 0.38 | 2.24 |
| APC4 | 7 | 0.91 | 1.88 | THIC | 17 | 0.37 | 2.19 |
| WFS1 | 15 | 0.90 | 1.56 | SPKAP | 8 | 0.36 | 2.91 |
| BGLR | 2 | 0.88 | 2.06 | PYR1 | 34 | 0.35 | 1.50 |
| DCXR | 5 | 0.84 | 1.33 | RHOF | 4 | 0.35 | 1.55 |
| VPP1 | 35 | 0.84 | 1.34 | AASS | 5 | 0.34 | 1.68 |
| VTNC | 2 | 0.83 | 2.01 | FHL1 | 3 | 0.33 | 1.35 |
| HEM2 | 13 | 0.82 | 4.63 | DYHC2 | 13 | 0.33 | 1.64 |
| HERC2 | 14 | 0.81 | 1.92 | WDR81 | 10 | 0.32 | 1.39 |
| HDHD3 | 7 | 0.80 | 2.09 | AT2B1 | 40 | 0.32 | 1.49 |

| | | | | | | | |
|---|---|---|---|---|---|---|---|
| PLRG1 | 3 | 0.80 | 2.49 | GANC | 2 | 0.32 | 2.11 |
| NCKPL | 2 | 0.78 | 1.75 | LYST | 18 | 0.31 | 1.74 |
| ADCY1 | 3 | 0.77 | 1.38 | GIPC1 | 13 | 0.30 | 1.94 |
| EPHA7 | 3 | 0.77 | 2.22 | E41L1 | 59 | 0.30 | 2.76 |
| DGKE | 5 | 0.76 | 1.46 | ATG2A | 8 | 0.29 | 2.21 |
| ADCY2 | 4 | 0.74 | 1.38 | FAS | 100 | 0.29 | 1.45 |
| DGKG | 9 | 0.74 | 1.68 | U520 | 58 | 0.29 | 1.45 |
| ACM1 | 2 | 0.73 | 1.41 | EPG5 | 12 | 0.28 | 1.43 |
| SYWM | 4 | 0.72 | 2.45 | SHIP2 | 7 | 0.27 | 1.32 |
| LCLT1 | 2 | 0.72 | 1.34 | PISD | 6 | 0.27 | 1.60 |
| ZMYM5 | 2 | 0.71 | 2.59 | C1TM | 34 | 0.26 | 1.34 |
| DHYS | 5 | 0.71 | 1.50 | PITC1 | 7 | 0.26 | 1.90 |
| VP13C | 40 | 0.70 | 1.39 | SPRY4 | 6 | 0.25 | 2.43 |
| CARL1 | 3 | 0.70 | 1.35 | ODR4 | 2 | 0.25 | 1.30 |
| KPCI | 3 | 0.70 | 1.90 | RAB2B | 4 | 0.25 | 2.03 |
| SYAM | 14 | 0.69 | 1.85 | BAZ1B | 4 | 0.24 | 1.90 |
| S2529 | 4 | 0.68 | 2.40 | FAIM1 | 3 | 0.24 | 2.10 |
| BRE1A | 8 | 0.68 | 1.30 | YBOX1 | 6 | 0.23 | 1.31 |
| DHB8 | 6 | 0.68 | 1.51 | IFT25 | 2 | 0.23 | 2.25 |
| SCN8A | 4 | 0.67 | 1.43 | CBPC1 | 6 | 0.23 | 1.55 |
| NMDZ1 | 17 | 0.67 | 1.39 | SMCR8 | 12 | 0.22 | 1.47 |
| RCC2 | 5 | 0.66 | 1.51 | M3K4 | 7 | 0.22 | 1.72 |
| APOE | 25 | 0.65 | 2.54 | RS9 | 17 | 0.22 | 1.77 |
| PTN6 | 3 | 0.65 | 2.26 | MLEC | 8 | 0.22 | 2.04 |
| GRM1 | 5 | 0.64 | 2.26 | HCFC1 | 10 | 0.22 | 1.32 |
| GSHR | 12 | 0.64 | 1.63 | FRY | 27 | 0.22 | 1.38 |
| PLTP | 5 | 0.61 | 2.02 | ABR | 28 | 0.22 | 1.46 |
| NGLY1 | 5 | 0.61 | 2.03 | RM24 | 4 | 0.21 | 1.40 |
| S38A3 | 4 | 0.61 | 1.43 | HD | 61 | 0.21 | 1.56 |
| BLTP1 | 20 | 0.60 | 2.48 | HECW1 | 13 | 0.21 | 1.31 |
| DIRC2 | 2 | 0.60 | 2.02 | SNF8 | 8 | 0.21 | 2.35 |
| VGLU1 | 8 | 0.60 | 1.55 | JAK1 | 4 | 0.20 | 2.47 |
| GRM3 | 13 | 0.60 | 1.41 | RL7 | 20 | 0.20 | 1.40 |
| BAD | 2 | 0.60 | 1.84 | KCC2B | 19 | 0.20 | 1.94 |
| TEN2 | 21 | 0.59 | 1.32 | DJC10 | 5 | 0.19 | 2.17 |
| IRGQ | 12 | 0.59 | 2.53 | GLCNE | 4 | 0.18 | 1.46 |
| GRM2 | 9 | 0.58 | 1.33 | PPIL1 | 4 | 0.18 | 1.40 |
| MYCB2 | 29 | 0.58 | 1.40 | DJB11 | 7 | 0.18 | 1.84 |
| ABCA5 | 4 | 0.55 | 1.34 | RB33B | 4 | 0.18 | 1.31 |
| PALM3 | 4 | 0.55 | 1.59 | ADDG | 34 | 0.18 | 1.64 |
| NMDE2 | 24 | 0.54 | 1.48 | SAHH3 | 13 | 0.17 | 1.72 |
| DGLA | 13 | 0.53 | 1.36 | UBE4B | 15 | 0.14 | 1.58 |
| RL27 | 5 | 0.53 | 1.33 | IF4A3 | 16 | 0.13 | 2.91 |

| | | | | | | | |
|---|---|---|---|---|---|---|---|
| M4K5 | 2 | 0.53 | 1.77 | TXND9 | 4 | 0.13 | 4.28 |
| KBTB3 | 2 | 0.53 | 1.58 | TRRAP | 13 | 0.13 | 1.38 |
| GABR2 | 15 | 0.53 | 1.39 | RLGPB | 14 | 0.13 | 1.59 |
| DPCD | 4 | 0.52 | 1.69 | ALG2 | 15 | 0.12 | 2.44 |
| NDE1 | 3 | 0.52 | 1.43 | RL13 | 10 | 0.08 | 1.36 |

Table 2

Significantly downregulated proteins in brain cortex of *5x-FAD* female mice

| **Gene Symbol** | **No. of unique peptides** | **$Log_2$ of fold change** | **$-Log_{10}$ of P-value** | | **No. of unique peptides** | **$Log_2$ of fold change** | **$-Log_{10}$ of P-value** |
|---|---|---|---|---|---|---|---|
| MSRB2 | 4 | -4.73 | 5.12 | ZN598 | 3 | -0.33 | 2.04 |
| CKLF5 | 2 | -2.44 | 2.47 | BIG2 | 24 | -0.33 | 1.94 |
| MOBP | 6 | -2.17 | 3.60 | ODP2 | 22 | -0.33 | 1.39 |
| A1AT4 | 4 | -2.09 | 1.51 | CA2D1 | 32 | -0.32 | 1.54 |
| F177A | 5 | -1.91 | 3.71 | SURF1 | 6 | -0.32 | 1.49 |
| APCL | 2 | -1.63 | 1.96 | OXSR1 | 8 | -0.32 | 1.35 |
| MOG | 13 | -1.60 | 3.03 | STRC | 2 | -0.32 | 1.79 |
| MAG | 18 | -1.54 | 2.63 | THY1 | 8 | -0.32 | 1.74 |
| CROCC | 62 | -1.44 | 3.03 | ITA1 | 4 | -0.32 | 1.66 |
| ANLN | 10 | -1.44 | 2.25 | GAB1 | 4 | -0.32 | 1.72 |
| IGHM | 4 | -1.44 | 1.64 | LMTK3 | 16 | -0.32 | 1.51 |
| TBCD1 | 2 | -1.41 | 1.72 | PLSI | 7 | -0.31 | 2.18 |
| CAH14 | 2 | -1.28 | 2.40 | APT | 5 | -0.31 | 1.78 |
| OPALI | 2 | -1.27 | 3.21 | GGT7 | 14 | -0.31 | 1.41 |
| PIANP | 2 | -1.06 | 1.81 | WNK2 | 23 | -0.31 | 1.63 |
| CN37 | 33 | -1.01 | 3.05 | SBP1 | 15 | -0.30 | 1.64 |
| ALR | 3 | -0.98 | 1.45 | ZO2 | 23 | -0.30 | 2.60 |
| NAA30 | 3 | -0.98 | 3.47 | MA7D2 | 18 | -0.30 | 2.38 |
| DUS15 | 6 | -0.95 | 2.57 | SPART | 5 | -0.30 | 2.73 |
| XPP3 | 2 | -0.92 | 1.65 | MMSA | 27 | -0.30 | 1.39 |
| IAH1 | 3 | -0.90 | 1.78 | ATPG | 23 | -0.30 | 2.86 |
| SIR2 | 19 | -0.89 | 2.94 | I5P1 | 8 | -0.30 | 1.74 |
| MYO1D | 29 | -0.89 | 2.72 | 2ABA | 12 | -0.29 | 1.31 |
| AL3B1 | 6 | -0.86 | 1.62 | MAP6 | 88 | -0.29 | 1.39 |
| AKTS1 | 2 | -0.80 | 2.05 | LPPRC | 47 | -0.29 | 1.31 |
| MUC18 | 7 | -0.78 | 2.35 | ALDH2 | 19 | -0.29 | 2.03 |
| DIAP1 | 14 | -0.77 | 1.48 | DNJB4 | 8 | -0.29 | 1.44 |

| | | | | | | | |
|---|---|---|---|---|---|---|---|
| EFNB3 | 7 | -0.76 | 3.13 | CADM3 | 9 | -0.29 | 1.61 |
| GLUCM | 9 | -0.75 | 1.58 | CEND | 15 | -0.29 | 1.56 |
| GLSL | 3 | -0.75 | 1.68 | ODPX | 19 | -0.28 | 1.70 |
| UFM1 | 2 | -0.74 | 1.80 | BIN1 | 32 | -0.28 | 1.35 |
| PPBT | 7 | -0.73 | 1.41 | CNTN2 | 20 | -0.28 | 1.71 |
| JAM3 | 7 | -0.68 | 1.66 | AASD1 | 13 | -0.28 | 1.43 |
| MBP | 21 | -0.68 | 1.32 | TTC9A | 6 | -0.28 | 1.74 |
| TYRO3 | 7 | -0.68 | 3.07 | ASPH2 | 2 | -0.27 | 2.13 |
| TOIP1 | 3 | -0.67 | 2.30 | PLCL1 | 19 | -0.27 | 1.38 |
| PPR3E | 2 | -0.67 | 2.89 | MTUS2 | 7 | -0.27 | 1.76 |
| LGI3 | 11 | -0.66 | 2.20 | SCMC2 | 7 | -0.27 | 1.48 |
| SYJ2B | 7 | -0.64 | 1.70 | MYPT1 | 25 | -0.27 | 1.49 |
| PLXA4 | 27 | -0.63 | 4.29 | TMOD1 | 17 | -0.27 | 1.32 |
| CRBB1 | 3 | -0.63 | 1.73 | MPRD | 3 | -0.26 | 1.49 |
| CLIC5 | 2 | -0.62 | 2.28 | IMPCT | 15 | -0.26 | 1.36 |
| LYAG | 19 | -0.62 | 1.33 | SYNPO | 40 | -0.26 | 1.40 |
| DAAM2 | 12 | -0.61 | 1.32 | STIM1 | 9 | -0.26 | 2.26 |
| ERMIN | 14 | -0.61 | 2.80 | RGS17 | 3 | -0.26 | 1.43 |
| RHOG | 8 | -0.60 | 1.57 | LUZP1 | 14 | -0.25 | 1.40 |
| SHPS1 | 16 | -0.60 | 2.74 | CPEB2 | 2 | -0.25 | 1.31 |
| NDRG1 | 14 | -0.59 | 2.76 | RIPR1 | 9 | -0.25 | 1.33 |
| MYG1 | 7 | -0.59 | 1.48 | HIP1 | 21 | -0.25 | 1.31 |
| CRYAB | 11 | -0.59 | 1.39 | PDC6I | 33 | -0.25 | 1.58 |
| OTUD4 | 3 | -0.59 | 1.98 | CDKL5 | 16 | -0.25 | 2.90 |
| HS71A | 10 | -0.57 | 1.91 | CAMP1 | 23 | -0.25 | 1.42 |
| CSEN | 4 | -0.56 | 1.52 | MON1A | 6 | -0.25 | 1.53 |
| CK068 | 3 | -0.55 | 2.11 | ULA1 | 15 | -0.24 | 1.34 |
| AL4A1 | 20 | -0.53 | 2.00 | AAK1 | 41 | -0.24 | 1.61 |
| TENS1 | 17 | -0.53 | 2.69 | RFTN1 | 6 | -0.24 | 1.33 |
| CLC2L | 4 | -0.52 | 1.65 | TTC1 | 5 | -0.24 | 1.54 |
| TUTLB | 4 | -0.51 | 1.32 | KCC1A | 6 | -0.23 | 2.44 |
| NDUAA | 16 | -0.51 | 1.76 | ABD12 | 17 | -0.23 | 1.58 |
| PNKP | 3 | -0.51 | 1.42 | ODO1 | 53 | -0.23 | 2.04 |
| SYVM | 7 | -0.51 | 1.93 | AK1A1 | 17 | -0.23 | 1.35 |
| ADA10 | 4 | -0.50 | 1.34 | SGTB | 5 | -0.23 | 1.44 |
| CP110 | 2 | -0.50 | 2.47 | L1CAM | 27 | -0.23 | 1.46 |
| EXOG | 10 | -0.50 | 1.79 | CNTN1 | 61 | -0.22 | 1.38 |
| ACOT2 | 4 | -0.49 | 1.57 | CADH6 | 7 | -0.22 | 1.80 |
| ENPP6 | 9 | -0.49 | 2.44 | GMPPA | 8 | -0.22 | 1.99 |
| NECT1 | 9 | -0.49 | 1.39 | RHG32 | 30 | -0.22 | 1.34 |
| PLCH1 | 2 | -0.49 | 1.33 | OGFR | 8 | -0.22 | 1.64 |
| PURA2 | 13 | -0.49 | 1.36 | AATC | 27 | -0.22 | 1.37 |
| CADM4 | 9 | -0.49 | 1.45 | SCO1 | 5 | -0.21 | 1.44 |

| | | | | | | | |
|---|---|---|---|---|---|---|---|
| CAN2 | 22 | -0.48 | 1.95 | RABL6 | 18 | -0.21 | 1.32 |
| STX4 | 9 | -0.48 | 1.82 | USE1 | 3 | -0.21 | 2.13 |
| THYN1 | 2 | -0.47 | 1.47 | AL1B1 | 15 | -0.21 | 1.62 |
| AL7A1 | 20 | -0.46 | 2.56 | GUAD | 25 | -0.21 | 2.36 |
| SYYC | 27 | -0.45 | 1.59 | ODO2 | 16 | -0.21 | 1.60 |
| BPNT1 | 7 | -0.44 | 1.40 | CNTN3 | 7 | -0.21 | 2.71 |
| CNTFR | 5 | -0.44 | 1.33 | SGIP1 | 46 | -0.21 | 1.96 |
| SDHB | 14 | -0.44 | 2.13 | ENOA | 38 | -0.20 | 1.62 |
| BABA1 | 3 | -0.43 | 1.79 | MAP7 | 9 | -0.20 | 1.52 |
| AT5F1 | 28 | -0.43 | 1.70 | NP1L1 | 13 | -0.20 | 1.99 |
| MILK1 | 2 | -0.43 | 3.51 | REPS1 | 11 | -0.20 | 1.86 |
| CLYBL | 15 | -0.43 | 3.08 | PUR8 | 13 | -0.20 | 1.31 |
| QCR1 | 24 | -0.43 | 1.37 | DCA11 | 7 | -0.20 | 1.60 |
| ZNT9 | 6 | -0.42 | 1.84 | OTU7B | 2 | -0.20 | 1.52 |
| PLXD1 | 18 | -0.42 | 3.00 | AMPD2 | 27 | -0.20 | 1.44 |
| ATPA | 48 | -0.42 | 2.53 | UPP | 2 | -0.20 | 1.40 |
| 4-Sep | 14 | -0.41 | 1.88 | EPN2 | 19 | -0.19 | 1.34 |
| SNX6 | 15 | -0.41 | 1.69 | AIFM1 | 25 | -0.18 | 1.52 |
| ASPH1 | 5 | -0.41 | 3.15 | ETFD | 17 | -0.18 | 1.58 |
| ATPB | 47 | -0.41 | 3.16 | LYRIC | 21 | -0.18 | 1.60 |
| YTHD3 | 2 | -0.41 | 2.01 | LA | 17 | -0.18 | 1.56 |
| CORO6 | 5 | -0.40 | 2.90 | KAP1 | 6 | -0.18 | 1.60 |
| GSTM7 | 6 | -0.40 | 3.73 | VATC1 | 40 | -0.18 | 2.39 |
| VTI1B | 7 | -0.39 | 1.60 | ASPC1 | 14 | -0.17 | 1.99 |
| PKHA6 | 9 | -0.39 | 1.47 | ODPA | 30 | -0.17 | 1.42 |
| PHLB1 | 6 | -0.39 | 1.69 | SH3G2 | 23 | -0.17 | 1.35 |
| TTBK1 | 11 | -0.39 | 1.53 | PICK1 | 5 | -0.17 | 1.43 |
| CLIC4 | 13 | -0.39 | 1.71 | SEPT7 | 34 | -0.16 | 1.47 |
| AFTIN | 6 | -0.39 | 2.97 | ALDOA | 32 | -0.16 | 1.61 |
| PYGL | 9 | -0.38 | 1.95 | MA7D1 | 26 | -0.16 | 2.25 |
| STXB3 | 7 | -0.38 | 2.37 | 8-Sep | 18 | -0.16 | 1.32 |
| SEC62 | 3 | -0.37 | 1.72 | NEUFC | 2 | -0.15 | 1.42 |
| TACC2 | 7 | -0.37 | 1.43 | PI42C | 12 | -0.15 | 2.40 |
| SERC | 16 | -0.36 | 1.57 | 11-Sep | 13 | -0.15 | 1.56 |
| WNK1 | 18 | -0.36 | 1.99 | NED4L | 21 | -0.15 | 1.39 |
| C2D1A | 10 | -0.36 | 2.68 | PRS6B | 19 | -0.15 | 1.32 |
| NOP16 | 2 | -0.36 | 1.57 | MAGI1 | 15 | -0.15 | 1.42 |
| PAIP1 | 3 | -0.36 | 1.61 | ANXA7 | 15 | -0.15 | 2.65 |
| CNNM1 | 8 | -0.36 | 1.37 | BECN1 | 6 | -0.14 | 1.73 |
| ACAD9 | 28 | -0.36 | 1.88 | PURA | 16 | -0.14 | 1.33 |
| RT27 | 9 | -0.36 | 1.49 | CHMP3 | 10 | -0.14 | 2.19 |
| SDHA | 35 | -0.36 | 2.33 | SEPT5 | 18 | -0.14 | 1.43 |
| CY1 | 12 | -0.35 | 1.37 | CNTP2 | 31 | -0.13 | 1.47 |

| | | | | | | | |
|---|---|---|---|---|---|---|---|
| AKCL2 | 10 | -0.35 | 1.67 | CAMP3 | 21 | -0.13 | 1.53 |
| NEUM | 40 | -0.35 | 1.31 | TOM1 | 12 | -0.13 | 1.33 |
| LRC47 | 20 | -0.35 | 1.47 | PCBP1 | 14 | -0.13 | 1.63 |
| PCY1A | 3 | -0.35 | 1.42 | PGRC2 | 6 | -0.13 | 1.39 |
| LRFN5 | 4 | -0.35 | 2.29 | MAGI2 | 19 | -0.12 | 1.48 |
| AIMP2 | 7 | -0.35 | 1.95 | IDH3A | 19 | -0.12 | 2.76 |
| MINY1 | 3 | -0.34 | 2.50 | HNRPQ | 20 | -0.12 | 1.37 |
| NTNG2 | 4 | -0.34 | 1.35 | RADI | 19 | -0.11 | 1.30 |
| AB17B | 3 | -0.34 | 1.59 | NECP1 | 12 | -0.11 | 1.49 |
| AFG32 | 29 | -0.34 | 1.44 | HNRH2 | 7 | -0.11 | 2.80 |
| WNK3 | 9 | -0.34 | 1.35 | IQGA1 | 18 | -0.11 | 1.88 |
| GSHB | 11 | -0.34 | 1.48 | RNZ2 | 7 | -0.10 | 1.55 |
| TMM65 | 10 | -0.34 | 1.45 | LRSM1 | 13 | -0.09 | 1.44 |
| CSK21 | 18 | -0.34 | 2.18 | E41L2 | 40 | -0.09 | 1.50 |
| RHOB | 3 | -0.34 | 1.44 | UBP8 | 9 | -0.08 | 1.56 |
| LGI2 | 9 | -0.34 | 4.17 | GGPPS | 3 | -0.08 | 1.64 |
| STML2 | 8 | -0.34 | 2.21 | HMOX2 | 16 | -0.08 | 1.76 |
| ZO1 | 35 | -0.33 | 1.72 | ATX2L | 20 | -0.06 | 1.48 |

**References**


1. International, A.s.D. *Dementia Statistics* 2020 15 April 2024]; Available from: https://www.alzint.org/about/dementia-facts-figures/dementia-statistics/#:~:text=Numbers%20of%20people%20with%20dementia,will%20be%20in%20developing%20countries

2. Association, A.s. *Inside the Brain: A tour of how the mind works* 2020 15 April 2024]; Available from: https://www.alz.org/alzheimers-dementia/what-is-alzheimers/brain_tour?lang=en-US#:~:text=With%20each%20heartbeat%2C%20arteries%20carry,of%20the%20fuel%20and%20oxygen.

3. Association, A.s. *Alzheimer's Disease Facts and Figures*. 2024 15 April 2024]; Available from: https://www.alz.org/alzheimers-dementia/facts-figures#:~:text=More%20than%206%20million%20Americans%20of%20all%20ages%20have%20Alzheimer's,older%20(10.7%25)%20has%20Alzheimer's.

4. Rice, V.H. *Arizona Is Getting Older...But so Is the U.S.* 2020 15 April 2024]; Available from: https://www.azeconomy.org/2020/07/economy/arizona-is-getting-older-and-so-is-the-u-s/.

5. Organization, W.H. *Dementia* 2023 15 April 2024]; Available from: https://www.who.int/news-room/fact-sheets/detail/dementia#:~:text=Alzheimer%20disease%20is%20the%20most%20common%20form%20and%20may%20contribute,frontal%20lobe%20of%20the%20brain.

6. Seeman, P. and N. Seeman, *Alzheimer's disease: β-amyloid plaque formation in human brain.* Synapse, 2011. **65**(12): p. 1289-1297.

7. Friedrich, R.P., et al., *Mechanism of amyloid plaque formation suggests an intracellular basis of Aβ pathogenicity.* Proceedings of the National Academy of Sciences, 2010. **107**(5): p. 1942-1947.

8. Gouras, G.K., T.T. Olsson, and O. Hansson, *β-Amyloid peptides and amyloid plaques in Alzheimer's disease.* Neurotherapeutics, 2015. **12**(1): p. 3-11.

9. Braak, H., et al., *Neuropathological hallmarks of Alzheimer's and Parkinson's diseases.* Progress in brain research, 1998. **117**: p. 267-285.

10. Gong, C.-X. and K. Iqbal, *Hyperphosphorylation of microtubule-associated protein tau: a promising therapeutic target for Alzheimer disease.* Current medicinal chemistry, 2008. **15**(23): p. 2321-2328.
11. Kregel, K.C. and H.J. Zhang, *An integrated view of oxidative stress in aging: basic mechanisms, functional effects, and pathological considerations.* American Journal of Physiology-Regulatory, Integrative and Comparative Physiology, 2007. **292**(1): p. R18-R36.
12. Parodi-Rullán, R., J.Y. Sone, and S. Fossati, *Endothelial mitochondrial dysfunction in cerebral amyloid angiopathy and Alzheimer's disease.* Journal of Alzheimer's disease, 2019. **72**(4): p. 1019-1039.
13. Pires, P.W., et al., *The effects of hypertension on the cerebral circulation.* American Journal of Physiology-Heart and Circulatory Physiology, 2013. **304**(12): p. H1598-H1614.
14. Polk, F.D., et al., *Endothelial KIR2 channel dysfunction in aged cerebral parenchymal arterioles.* American Journal of Physiology-Heart and Circulatory Physiology, 2023. **325**(6): p. H1360-H1372.
15. Erö, C., et al., *A cell atlas for the mouse brain.* Frontiers in neuroinformatics, 2018. **12**: p. 84.
16. Weller, R.O., D. Boche, and J.A. Nicoll, *Microvasculature changes and cerebral amyloid angiopathy in Alzheimer's disease and their potential impact on therapy.* Acta neuropathologica, 2009. **118**: p. 87-102.
17. Weller, R.O., et al., *Lymphatic drainage of the brain and the pathophysiology of neurological disease.* Acta neuropathologica, 2009. **117**: p. 1-14.
18. Tarantini, S., et al., *Impaired neurovascular coupling in aging and Alzheimer's disease: contribution of astrocyte dysfunction and endothelial impairment to cognitive decline.* Experimental gerontology, 2017. **94**: p. 52-58.
19. Toth, P., et al., *Functional vascular contributions to cognitive impairment and dementia: mechanisms and consequences of cerebral autoregulatory dysfunction, endothelial impairment, and neurovascular uncoupling in aging.* American Journal of Physiology-Heart and Circulatory Physiology, 2017. **312**(1): p. H1-H20.

20. Gu, L., et al., *Myelin changes at the early stage of 5XFAD mice.* Brain research bulletin, 2018. **137**: p. 285-293.
21. Huang, W.J., X. Zhang, and W.W. Chen, *Role of oxidative stress in Alzheimer's disease.* Biomedical reports, 2016. **4**(5): p. 519-522.
22. Chen, X., C. Guo, and J. Kong, *Oxidative stress in neurodegenerative diseases☆.* Neural regeneration research, 2012. **7**(5): p. 376-385.
23. Redza-Dutordoir, M. and D.A. Averill-Bates, *Activation of apoptosis signalling pathways by reactive oxygen species.* Biochimica et Biophysica Acta (BBA)-Molecular Cell Research, 2016. **1863**(12): p. 2977-2992.
24. Malinski, T., *Nitric oxide and nitroxidative stress in Alzheimer's disease.* Journal of Alzheimer's disease, 2007. **11**(2): p. 207-218.
25. Christen, Y., *Oxidative stress and Alzheimer disease.* The American journal of clinical nutrition, 2000. **71**(2): p. 621S-629S.
26. Smith, M.A., et al., *Oxidative stress in Alzheimer's disease.* Biochimica et Biophysica Acta (BBA)-Molecular Basis of Disease, 2000. **1502**(1): p. 139-144.
27. Burwell, L.S., et al., *Direct evidence for S-nitrosation of mitochondrial complex I.* Biochemical Journal, 2006. **394**(3): p. 627-634.
28. Chen, Z. and C. Zhong, *Oxidative stress in Alzheimer's disease.* Neuroscience bulletin, 2014. **30**: p. 271-281.
29. Spencer, N.G., et al., *Quantitative evaluation of MRI and histological characteristics of the 5xFAD Alzheimer mouse brain.* Neuroimage, 2013. **76**: p. 108-115.
30. Förstermann, U. and W.C. Sessa, *Nitric oxide synthases: regulation and function.* European heart journal, 2012. **33**(7): p. 829-837.
31. Cau, S.B., F.S. Carneiro, and R.C. Tostes, *Differential modulation of nitric oxide synthases in aging: therapeutic opportunities.* Frontiers in physiology, 2012. **3**: p. 218.
32. Esposito, Z., et al., *Amyloid β, glutamate, excitotoxicity in Alzheimer's disease: are we on the right track?* CNS neuroscience & therapeutics, 2013. **19**(8): p. 549-555.
33. Hynd, M.R., H.L. Scott, and P.R. Dodd, *Glutamate-mediated excitotoxicity and neurodegeneration in Alzheimer's disease.* Neurochemistry international, 2004. **45**(5): p. 583-595.

34. Cheignon, C.m., et al., *Oxidative stress and the amyloid beta peptide in Alzheimer's disease.* Redox biology, 2018. **14**: p. 450-464.
35. Zahid, S., et al., *Differential S-nitrosylation of proteins in Alzheimer's disease.* Neuroscience, 2014. **256**: p. 126-136.
36. Bai, B., et al., *Deep multilayer brain proteomics identifies molecular networks in Alzheimer's disease progression.* Neuron, 2020. **105**(6): p. 975-991. e7.
37. Papassotiropoulos, A., et al., *Genetics, transcriptomics, and proteomics of Alzheimer's disease.* Journal of Clinical Psychiatry, 2006. **67**(4): p. 652.
38. Dammer, E.B., et al., *Quantitative phosphoproteomics of Alzheimer's disease reveals cross-talk between kinases and small heat shock proteins.* Proteomics, 2015. **15**(2-3): p. 508-519.
39. Johnson, E.C., et al., *Large-scale deep multi-layer analysis of Alzheimer's disease brain reveals strong proteomic disease-related changes not observed at the RNA level.* Nature neuroscience, 2022. **25**(2): p. 213-225.
40. Askenazi, M., et al., *Compilation of reported protein changes in the brain in Alzheimer's disease.* Nature Communications, 2023. **14**(1): p. 4466.
41. Kim, D.K., et al., *Deep proteome profiling of the hippocampus in the 5XFAD mouse model reveals biological process alterations and a novel biomarker of Alzheimer's disease.* Experimental & molecular medicine, 2019. **51**(11): p. 1-17.
42. Rangaraju, S., et al., *Quantitative proteomics of acutely-isolated mouse microglia identifies novel immune Alzheimer's disease-related proteins.* Molecular neurodegeneration, 2018. **13**: p. 1-19.
43. Zhao, Q.-F., J.-T. Yu, and L. Tan, *S-Nitrosylation in Alzheimer's disease.* Molecular neurobiology, 2015. **51**: p. 268-280.
44. Sun, J., C. Steenbergen, and E. Murphy, *S-nitrosylation: NO-related redox signaling to protect against oxidative stress.* Antioxidants & redox signaling, 2006. **8**(9-10): p. 1693-1705.
45. Kruse, R., et al., *Characterization of the CLASP2 Protein Interaction Network Identifies SOGA1 as a Microtubule-Associated Protein.* Mol Cell Proteomics, 2017. **16**(10): p. 1718-1735.

46. Parker, S.S., et al., *Insulin Induces Microtubule Stabilization and Regulates the Microtubule Plus-end Tracking Protein Network in Adipocytes.* Mol Cell Proteomics, 2019. **18**(7): p. 1363-1381.
47. Tyanova, S. and J. Cox, *Perseus: A Bioinformatics Platform for Integrative Analysis of Proteomics Data in Cancer Research.* Methods Mol Biol, 2018. **1711**: p. 133-148.
48. Tyanova, S., et al., *The Perseus computational platform for comprehensive analysis of (prote)omics data.* Nat Methods, 2016. **13**(9): p. 731-40.
49. Huang da, W., B.T. Sherman, and R.A. Lempicki, *Systematic and integrative analysis of large gene lists using DAVID bioinformatics resources.* Nat Protoc, 2009. **4**(1): p. 44-57.
50. Hong, I., et al., *Quantitative proteomic analysis of the hippocampus in the 5XFAD mouse model at early stages of Alzheimer's disease pathology.* Journal of Alzheimer's Disease, 2013. **36**(2): p. 321-334.
51. Maitre, M., et al., *Myelin in Alzheimer's disease: culprit or bystander?* Acta Neuropathologica Communications, 2023. **11**(1): p. 56.
52. Papuć, E. and K. Rejdak, *The role of myelin damage in Alzheimer's disease pathology.* Archives of Medical Science, 2018. **16**(2): p. 345-341.
53. Tagawa, K., et al., *Comprehensive phosphoproteome analysis unravels the core signaling network that initiates the earliest synapse pathology in preclinical Alzheimer's disease brain.* Human molecular genetics, 2015. **24**(2): p. 540-558.
54. Lu, X., et al., *Histone acetylation modifiers in the pathogenesis of Alzheimer's disease.* Frontiers in cellular neuroscience, 2015. **9**: p. 226.
55. Stilling, R.M. and A. Fischer, *The role of histone acetylation in age-associated memory impairment and Alzheimer's disease.* Neurobiology of learning and memory, 2011. **96**(1): p. 19-26.
56. Wang, R. and P.H. Reddy, *Role of glutamate and NMDA receptors in Alzheimer's disease.* Journal of Alzheimer's Disease, 2017. **57**(4): p. 1041-1048.
57. Mazzola, J.L. and M.A. Sirover, *Reduction of glyceraldehyde-3-phosphate dehydrogenase activity in Alzheimer's disease and in Huntington's disease fibroblasts.* Journal of neurochemistry, 2001. **76**(2): p. 442-449.

58. Shalova, I.N., et al., *Decrease of dehydrogenase activity of cerebral glyceraldehyde-3-phosphate dehydrogenase in different animal models of Alzheimer's disease.* Biochimica et Biophysica Acta (BBA)-General Subjects, 2007. **1770**(5): p. 826-832.
59. Atamna, H. and W.H. Frey II, *Mechanisms of mitochondrial dysfunction and energy deficiency in Alzheimer's disease.* Mitochondrion, 2007. **7**(5): p. 297-310.
60. Qu, J., et al., *S-nitrosylation of Cdk5: potential implications in amyloid-β-related neurotoxicity in Alzheimer disease.* Prion, 2012. **6**(4): p. 364-370.
61. Gu, L. and R.A. Robinson, *High-throughput endogenous measurement of S-nitrosylation in Alzheimer's disease using oxidized cysteine-selective cPILOT.* Analyst, 2016. **141**(12): p. 3904-3915.
62. Yang, Z. and K.K. Wang, *Glial fibrillary acidic protein: from intermediate filament assembly and gliosis to neurobiomarker.* Trends in neurosciences, 2015. **38**(6): p. 364-374.
63. Abdelhak, A., et al., *Blood GFAP as an emerging biomarker in brain and spinal cord disorders.* Nat Rev Neurol, 2022. **18**(3): p. 158-172.
64. Zhou, X., et al., *Isoform-specific effects of neuronal repression of the AMPK catalytic subunit on cognitive function in aged mice.* Aging (Albany NY), 2023. **15**(4): p. 932.
65. Kister, A. and I. Kister, *Overview of myelin, major myelin lipids, and myelin-associated proteins.* Frontiers in Chemistry, 2023. **10**: p. 1041961.
66. Cho, D.-H., et al., *S-nitrosylation of Drp1 mediates β-amyloid-related mitochondrial fission and neuronal injury.* Science, 2009. **324**(5923): p. 102-105.
67. Nakamura, T. and S.A. Lipton, *S-nitrosylation of critical protein thiols mediates protein misfolding and mitochondrial dysfunction in neurodegenerative diseases.* Antioxidants & redox signaling, 2011. **14**(8): p. 1479-1492.
68. Qu, J., et al., *S-Nitrosylation activates Cdk5 and contributes to synaptic spine loss induced by β-amyloid peptide.* Proceedings of the National Academy of Sciences, 2011. **108**(34): p. 14330-14335.
69. Andreyev, A.Y., et al., *Metabolic Bypass Rescues Aberrant S-nitrosylation-Induced TCA Cycle Inhibition and Synapse Loss in Alzheimer's Disease Human Neurons.* Advanced Science, 2024: p. 2306469.
70. Gomez, M.A.R. and M. Ibba, *Aminoacyl-tRNA synthetases.* Rna, 2020. **26**(8): p. 910-936.

71. Suzuki, T., *The expanding world of tRNA modifications and their disease relevance.* Nature Reviews Molecular Cell Biology, 2021. **22**(6): p. 375-392.
72. Zheng, W.-Q., et al., *Nitrosative stress inhibits aminoacylation and editing activities of mitochondrial threonyl-tRNA synthetase by S-nitrosation.* Nucleic Acids Research, 2020. **48**(12): p. 6799-6810.
73. Bizzozero, O.A., G. DeJesus, and T.A. Howard, *Exposure of rat optic nerves to nitric oxide causes protein S-nitrosation and myelin decompaction.* Neurochemical research, 2004. **29**: p. 1675-1685.
74. Smith, K.J., R. Kapoor, and P.A. Felts, *Demyelination: the role of reactive oxygen and nitrogen species.* Brain pathology, 1999. **9**(1): p. 69-92.
75. De, S., et al., *Phosphorylation of α-tubulin by protein kinase C stimulates microtubule dynamics in human breast cells.* Cytoskeleton, 2014. **71**(4): p. 257-272.
76. Sánchez, C., J. Dıaz-Nido, and J. Avila, *Phosphorylation of microtubule-associated protein 2 (MAP2) and its relevance for the regulation of the neuronal cytoskeleton function.* Progress in neurobiology, 2000. **61**(2): p. 133-168.
77. Yang, M., et al., *The role of microtubule-associated protein 1B in axonal growth and neuronal migration in the central nervous system ☆.* Neural Regeneration Research, 2012. **7**(11): p. 842-848.
78. Lordén, G., et al., *Enhanced activity of Alzheimer disease-associated variant of protein kinase Cα drives cognitive decline in a mouse model.* Nature communications, 2022. **13**(1): p. 7200.
79. Poulsen, H., et al., *Phosphorylation of the Na+, K+-ATPase and the H+, K+-ATPase.* FEBS letters, 2010. **584**(12): p. 2589-2595.
80. Geering, K., *Functional roles of Na, K-ATPase subunits.* Current opinion in nephrology and hypertension, 2008. **17**(5): p. 526-532.
81. Vitvitsky, V.M., et al., *Na+ and K+ ion imbalances in Alzheimer's disease.* Biochimica et Biophysica Acta (BBA)-Molecular Basis of Disease, 2012. **1822**(11): p. 1671-1681.
82. McDonough, A.A. and R.A. Farley, *Regulation of Na, K-ATPase activity.* Current opinion in nephrology and hypertension, 1993. **2**(5): p. 725-734.

83. Sun, L., et al., *The human brain acetylome reveals that decreased acetylation of mitochondrial proteins associates with Alzheimer's disease.* Journal of Neurochemistry, 2021. **158**(2): p. 282-296.

84. da Silva, J.F., et al., *Sex-specific mechanisms of cerebral microvascular BK (Ca) dysfunction in a mouse model of Alzheimer's disease.* bioRxiv, 2024.